Preprint typeset in JHEP style - HYPER VERSION

SLAC-PUB-14136
June 3, 2010

# RECO level $\sqrt{s}_{min}$ and subsystem $\sqrt{s}_{min}$: improved global inclusive variables for measuring the new physics mass scale in $\not{E}_T$ events at hadron colliders

**Partha Konar**
*Physics Department, University of Florida, Gainesville, FL 32611, USA*
*E-mail:* konar@phys.ufl.edu

**Kyoungchul Kong**
*Theoretical Physics Department, SLAC, Menlo Park, CA 94025, USA*
*E-mail:* kckong@slac.stanford.edu

**Konstantin T. Matchev**
*Physics Department, University of Florida, Gainesville, FL 32611, USA*
*E-mail:* matchev@phys.ufl.edu

**Myeonghun Park**
*Physics Department, University of Florida, Gainesville, FL 32611, USA*
*E-mail:* ishaed@phys.ufl.edu

Abstract: The variable $\sqrt{s}_{min}$ was originally proposed in [1] as a model-independent, global and fully inclusive measure of the new physics mass scale in missing energy events at hadron colliders. In the original incarnation of $\sqrt{s}_{min}$, however, the connection to the new physics mass scale was blurred by the effects of the underlying event, most notably initial state radiation and multiple parton interactions. In this paper we advertize two improved variants of the $\sqrt{s}_{min}$ variable, which overcome this problem. First we show that by evaluating the $\sqrt{s}_{min}$ variable at the RECO level, in terms of the reconstructed objects in the event, the effects from the underlying event are significantly diminished and the nice correlation between the peak in the $\sqrt{s}_{min}^{(reco)}$ distribution and the new physics mass scale is restored. Secondly, the underlying event problem can be avoided altogether when the $\sqrt{s}_{min}$ concept is applied to a subsystem of the event which does not involve any QCD jets. We supply an analytic formula for the resulting subsystem $\sqrt{s}_{min}^{(sub)}$ variable and show that its peak exhibits the usual correlation with the mass scale of the particles produced in the subsystem. Finally, we contrast $\sqrt{s}_{min}$ to other popular inclusive variables such as $H_T$, $M_{Tgen}$ and $M_{TTgen}$. We illustrate our discussion with several examples from supersymmetry, and with dilepton events from top quark pair production.

Keywords: Beyond Standard Model, Hadronic Colliders, Supersymmetry Phenomenology.

## Contents



## 1. Introduction and motivation

### 1.1 The need for a universal, global and inclusive mass variable

It is generally believed that missing energy signatures offer the best bet for discovering new physics Beyond the Standard Model (BSM) at colliders. This belief is reinforced by the dark matter puzzle - the Standard Model (SM) does not contain a suitable dark matter candidate. If dark matter particles are produced at colliders, they will be invisible in the detector, and will in principle lead to missing energy and missing momentum. However, at hadron colliders the total energy and longitudinal momentum of the event are unknown. Therefore, the production of any invisible particles can only be inferred from an imbalance in the total *transverse* momentum. The measured *missing* transverse momentum $\vec{\not{P}}_T$ then gives the sum of the transverse momenta of all invisible particles in the event.

Unfortunately, $\vec{\not{P}}_T$ is the only measured quantity directly related to the invisible particles. Without any further model-dependent assumptions, it is in general very difficult if not

impossible to make any definitive statements about the nature and properties of the missing particles. For example, leaving all theoretical prejudice aside, one would not be able to answer such basic and fundamental questions like [1–5]: How many invisible particles were produced in the event? Are all invisible particles SM neutrinos, or are there any new neutral, stable, weakly-interacting massive particles (WIMPs) among them? What are the masses of the new invisible particles? What are their spins? What are the masses of any (parent) particles which may have decayed to invisible particles?

The recent literature is abundant with numerous proposals[1] on how *under particular circumstances* one might be able to measure the masses of the invisible particles. Unfortunately, all of the proposed methods suffer from varying degrees of model-dependence[2]:

- *Limited applicability topology-wise.* Most methods are model-dependent in the sense that each method crucially relies on the assumption of a very specific event topology. One common flaw of all methods on the market is that they usually do not allow any SM neutrinos to enter the targeted event topology, and the missing energy is typically assumed to arise only as a result of the production of (two) new dark matter particles. Furthermore, each method has its own limitations. For example, the traditional invariant mass endpoint methods [10–20] require the identification of a sufficiently long cascade decay chain, with at least three successive two-body decays [21]. The polynomial methods of Refs. [22–29] also require such long decay chains and furthermore, the events must be symmetric, i.e. must have two *identical* decay chains per event, or else the decay chain must be even longer [21]. The recently popular $M_{T2}$ methods [30–39] do not require long decay chains [21], but typically assume that the parent particles are the same and decay to two identical invisible particles[3]. The limitations of the $M_{CT}$ methods [40–42] are rather similar. The kinematic cusp method [43] is limited to the so called "antler" event topology, which contains two symmetric one-step decay chains originating from a single $s$-channel resonance. In light of all these various assumptions, it is certainly desirable to have a *universal* method which can be applied to *any* event topology. To the best of our knowledge, the only such method in the literature is the one proposed in Ref. [1], where the $\sqrt{s}_{min}$ variable was first introduced. The $\sqrt{s}_{min}$ variable is defined in terms of the *total* energy $E$ and 3-momentum $\vec{P}$ observed in the event, and thus does not make any reference to the actual event topology. In this sense $\sqrt{s}_{min}$ is a *universal* variable which can be applied under any circumstances.

- *Limited applicability signature-wise.* As a rule, most of the proposed methods work well only if the corresponding signature contains some minimum number of high $p_T$ isolated leptons. Leptonic signatures have the twofold advantage of lower SM backgrounds and good lepton momentum measurement. The performance of the methods typically deteriorates as we lower the number of leptons in the signature. The most challenging

[1] See Ref. [6] for a recent review.

[2] Worse still, there are even fewer ideas for measuring the *spins* of the new particles in a truly model-independent fashion [7–9].

[3] See [3, 4] for a more general approach which avoids this assumption.

signature of multijets plus $\not\!\!E_T$ has rarely been studied in relation to mass and spin measurements (see, however [33, 44–47]). Unfortunately, at hadron colliders like the Tevatron and LHC, one typically expects strong production to dominate the new physics cross-sections, and this in turn guarantees the presence of some minimum number of jets in the signature. At the same time, a priori there are no theoretical arguments which would similarly guarantee the presence of any hard isolated leptons. Therefore, one would like to have a general, sufficiently inclusive method, which treats jets and leptons on an equal footing. The $\sqrt{s}_{min}$ method of Ref. [1] satisfies this requirement as well, since it does not differentiate between the type of reconstructed objects. In fact, the original proposal of Ref. [1] did not require any object reconstruction at all, and used (muon-corrected) calorimeter energy measurements to define the observed $E$ and $\vec{P}$ in the event.

- *Combinatorics problem.* Even if one correctly guesses the new physics event topology, and the signature happens to be abundant in hard isolated leptons, one still has to face the usual combinatorics problem of how to properly associate the reconstructed objects with the individual particles in the assumed event topology. Here we shall be careful to make the distinction between two different aspects of the combinatorics problem:

  - *Partitioning ambiguity.* As a prototypical example, consider a model of supersymmetry (SUSY) in which $R$-parity is conserved and the lightest supersymmetric particle (LSP) is neutral and stable. Each SUSY event contains two independent cascade decay chains, so first one must decide which reconstructed objects belong to the first decay chain and which belong to the second [32, 48]. However, a priori there are no guiding principles on how to do this partitioning into subsets. The decision is further complicated by the inevitable presence of jets from initial state radiation, which have nothing to do with the SUSY cascades [49]; by final state radiation, which modifies the assumed event topology; and by the occasional overlapping of jets [50].
  - *Ordering ambiguity.* Having separated the objects into two groups, one must still decide on the sequential ordering of the reconstructed objects along each decay chain. One well-known example of this problem is the ambiguity between the "near" and "far" lepton in the standard jet-lepton-lepton squark decay chain [20].

  The severity of either one of these two combinatorics problems depends on the type of signature — simple signatures resulting from short decay chains suffer from less combinatorics but tend to have larger SM backgrounds. By the same token, more complex signatures, which result from longer decay chains, are easier to see over the SM backgrounds, but very quickly run into severe combinatorial problems. Thus ideally one would like to have a method which treats *all* objects in the event in a fully inclusive manner, so that *neither of these two* combinatorial issues can ever arise at all. The $\sqrt{s}_{min}$ variable of Ref. [1] was proposed for exactly this reason, and is free of the partitioning *and* ordering combinatorial ambiguities.

- *Limited use of the available experimental information.* At hadron colliders, events with invisible particles in the final state present an additional challenge: the total energy and longitudinal momentum of the initial state in the event are unknown. On the other hand, the *transverse* momentum of the initial state is known, which has greatly motivated the use of *transverse* variables like the missing "transverse energy" $\not{E}_T$, the scalar sum of transverse momenta $H_T$, the transverse mass $M_T$, the stransverse mass $M_{T2}$ [30], the contransverse mass $M_{CT}$ [40], etc. An unsettling feature of a purely transverse kinematical approach is that it completely ignores the measured longitudinal momentum components of the visible particles. In principle, the longitudinal momenta also carry a certain amount of information about the underlying physics, although it is difficult to see immediately how this information can be utilized. (For example, one cannot take advantage of longitudinal momentum conservation, because the longitudinal momentum of the initial state is unknown.) By defining the $\sqrt{s}_{min}$ variable in a manifestly 1+3 Lorentz invariant way, Ref. [1] proposed one possible way to utilize the additional information encoded in the measured longitudinal momenta.

The above discussion makes it clear that the method of the $\sqrt{s}_{min}$ variable has several unique advantages over all other known methods: it is completely general and universal, is fully inclusive, and to the fullest extent makes use of the available experimental information. In spite of these advantages, the $\sqrt{s}_{min}$ variable has not yet found wide application. The one major perceived drawback of $\sqrt{s}_{min}$ is its sensitivity to initial state radiation (ISR) and/or multiple parton interactions (MPI) [1, 6, 51–53]. To see how this comes about, let us first review the formal definition of $\sqrt{s}_{min}$.

### 1.2 Definition of $\sqrt{s}_{min}$

Consider the most generic missing energy event topology shown in Fig. 1. As seen from the figure, in defining $\sqrt{s}_{min}$, one imagines a completely general setup – each event contains some number $n_{vis}$ of Standard Model (SM) particles $X_i$, $i = 1, 2, \ldots, n_{vis}$, which are *visible* in the detector, i.e. their energies and momenta are in principle measured. Examples of such visible SM particles are the basic reconstructed objects, e.g. jets, photons, electrons and muons. The visible particles $X_i$ are denoted in Fig. 1 with solid black lines and may originate either from ISR, or from the hard scattering and subsequent cascade decays (indicated with the green-shaded ellipse). In turn, the missing transverse momentum $\vec{\not{p}}_T$ arises from a certain number $n_{inv}$ of stable neutral particles $\chi_i$, $i = 1, 2, \ldots, n_{inv}$, which are *invisible* in the detector. In general, the set of invisible particles consists of some number $n_\chi$ of BSM particles (indicated with the red dashed lines), as well as some number $n_\nu = n_{inv} - n_\chi$ of SM neutrinos (denoted with the black dashed lines). As already mentioned earlier, the $\vec{\not{p}}_T$ measurement alone does not reveal the number $n_{inv}$ of missing particles, nor how many of them are neutrinos and how many are BSM (dark matter) particles. This general setup also allows the identities and the masses $m_i$ of the BSM invisible particles $\chi_i$, $(i = 1, 2, \ldots, n_\chi)$ in principle to be different, as in models with several *different* species of dark matter particles [54–57]. Of course, the

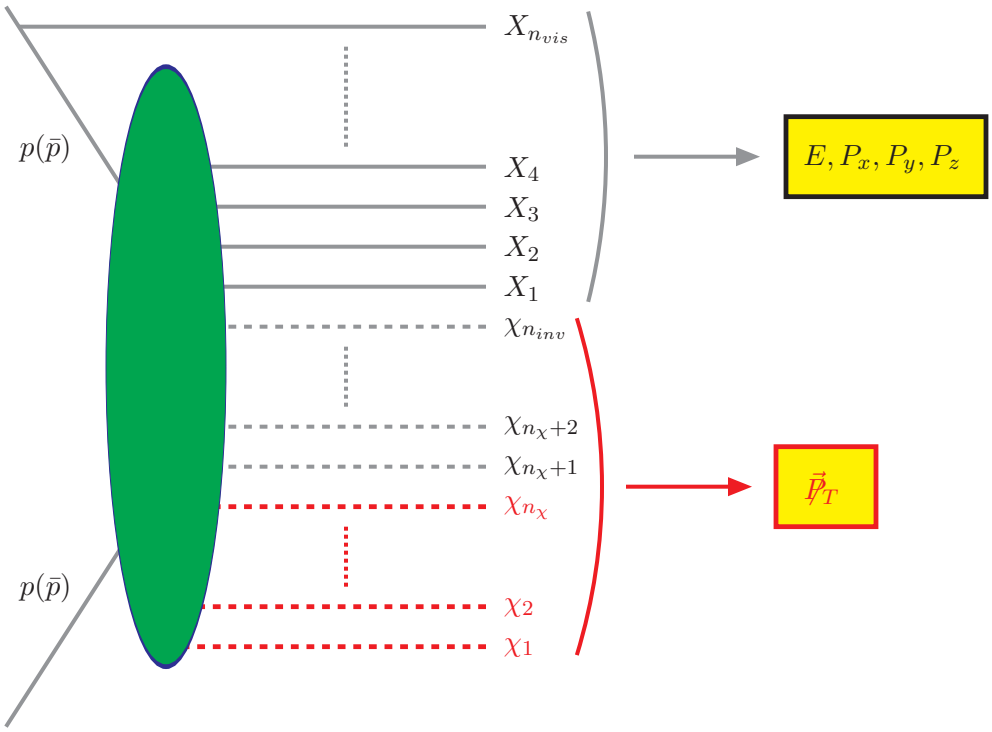


**Figure 1:** The generic event topology used to define the $\sqrt{s}_{min}$ variable in Ref. [1]. Black (red) lines correspond to SM (BSM) particles. The solid lines denote SM particles $X_i$, $i = 1, 2, \ldots, n_{vis}$, which are visible in the detector, e.g. jets, electrons, muons and photons. The SM particles may originate either from initial state radiation (ISR), or from the hard scattering and subsequent cascade decays (indicated with the green-shaded ellipse). The dashed lines denote neutral stable particles $\chi_i$, $i = 1, 2, \ldots, n_{inv}$, which are invisible in the detector. In general, the set of invisible particles consists of some number $n_\chi$ of BSM particles (indicated with the red dashed lines), as well as some number $n_\nu = n_{inv} - n_\chi$ of SM neutrinos (denoted with the black dashed lines). The identities and the masses $m_i$ of the BSM invisible particles $\chi_i$, $(i = 1, 2, \ldots, n_\chi)$ do not necessarily have to be all the same, i.e. we allow for the simultaneous production of several *different* species of dark matter particles. The global event variables describing the visible particles are: the total energy $E$, the transverse components $P_x$ and $P_y$ and the longitudinal component $P_z$ of the total visible momentum $\vec{P}$. The only experimentally available information regarding the invisible particles is the missing transverse momentum $\not{\vec{P}}_T$.

neutrino masses can be safely taken to be zero

$$m_i = 0, \quad \text{for } i = n_\chi + 1, n_\chi + 2, \ldots, n_{inv} \ . \tag{1.1}$$

Given this very general setup, Ref. [1] asked the following question: What is the *minimum* value $\sqrt{s}_{min}$ of the parton-level Mandelstam invariant mass variable $\sqrt{s}$ which is consistent with the observed visible 4-momentum vector $P^\mu \equiv (E, \vec{P})$? As it turned out, the answer to this question is given by the universal formula [1]

$$\sqrt{s}_{min}(\not{M}) \equiv \sqrt{E^2 - P_z^2} + \sqrt{\not{M}^2 + \not{P}_T^2} \ , \tag{1.2}$$

where the mass parameter $\not{M}$ is nothing but the total mass of all invisible particles in the event:

$$\not{M} \equiv \sum_{i=1}^{n_{inv}} m_i = \sum_{i=1}^{n_\chi} m_i \ , \tag{1.3}$$

and the second equality follows from the assumption of vanishing neutrino masses (1.1). The result (1.2) can be equivalently rewritten in a more symmetric form

$$\sqrt{s}_{min}(\not{M}) = \sqrt{M^2 + P_T^2} + \sqrt{\not{M}^2 + \not{P}_T^2} \tag{1.4}$$

in terms of the total visible invariant mass $M$ defined as

$$M^2 \equiv E^2 - P_x^2 - P_y^2 - P_z^2 \equiv E^2 - P_T^2 - P_z^2 \, . \tag{1.5}$$

Notice that in spite of the complete arbitrariness of the invisible particle sector at this point, the definition of $\sqrt{s}_{min}$ depends on a single unknown parameter $\not{M}$ - the *sum* of all the masses of the invisible particles in the event. For future reference, one should keep in mind that transverse momentum conservation at this point implies that

$$\vec{P}_T + \vec{\not{P}}_T = 0. \tag{1.6}$$

The main result from Ref. [1] was that in the absence of ISR and MPI, the peak in the $\sqrt{s}_{min}$ distribution nicely correlates with the mass threshold of the newly produced particles. This observation provides one generic relation between the total mass of the produced particles and the total mass $\not{M}$ of the invisible particles. Based on several SUSY examples involving fully hadronic signatures in symmetric as well as asymmetric topologies, Ref. [1] showed that the accuracy of this measurement rivals the one achieved with the more traditional $M_{T2}$ methods.

### 1.3 $\sqrt{s}_{min}$ and the underlying event problem

At the same time, it was also recognized that effects from the underlying event (UE), most notably ISR and MPI, severely jeopardize this measurement. The problem is that in the presence of the UE, the $\sqrt{s}_{min}$ variable would be measuring *the total* energy of the full system shown in Fig. 1, while for studying any new physics we are mostly interested in the energy of the hard scattering, as represented by the green-shaded ellipse in Fig. 1. The inclusion of the UE causes a drastic shift of the peak of the $\sqrt{s}_{min}$ distribution to higher values, often by as much as a few TeV [1, 51, 52]. As a result, it appeared that unless effects from the underlying event could somehow be compensated for, the proposed measurement of the $\sqrt{s}_{min}$ peak would be of no practical value.

The main purpose of this paper is to propose two fresh new approaches to dealing with the underlying event problem which has plagued the $\sqrt{s}_{min}$ variable and prevented its more widespread use in hadron collider physics applications. But before we discuss the two new ideas put forth in this paper, we first briefly mention the two existing proposals in the literature on how to deal with the underlying event problem.

First, it was recognized in Ref. [1] that the contributions from the underlying event tend to be in the forward region, i.e. at large values of $|\eta|$. Correspondingly, by choosing a suitable cut $|\eta| < \eta_{max}$, designed to eliminate contributions from the very forward regions, one could in principle restore the proper behavior of the $\sqrt{s}_{min}$ distribution [1]. Unfortunately, there are no a priori guidelines on how to choose the appropriate value of $\eta_{max}$, therefore this approach introduces an uncontrollable systematic error and has not been pursued further in the literature.

An alternative approach was proposed in Refs. [51, 52], which pointed out that the ISR effects on $\sqrt{s}_{min}$ are in principle calculable in QCD from first principles. The calculations presented in Refs. [51, 52] could then be used to "unfold" the ISR effects and correct for the shift in the peak of the $\sqrt{s}_{min}$ distribution. Unfortunately, in this analytical approach, the MPI effects would still be unaccounted for, and would have to be modeled and validated separately by some other means. While such an approach may eventually bear fruit at some point in the future, we shall not pursue it here.

We see that, for one reason or another, both of these strategies appear unsatisfactory. Therefore, here we shall pursue two different approaches. We shall propose two new variants of the $\sqrt{s}_{min}$ variable, which we label $\sqrt{s}^{(reco)}_{min}$ and $\sqrt{s}^{(sub)}_{min}$ and define in Secs. 2 and 3, correspondingly. We illustrate the properties of these two variables with several examples in Secs. 4-6. These examples will show that both $\sqrt{s}^{(reco)}_{min}$ and $\sqrt{s}^{(sub)}_{min}$ are unharmed by the effects from the underlying event, thus resurrecting the original idea of Ref. [1] to use the peak in the $\sqrt{s}_{min}$ distribution as a first, quick, model-independent estimate of the new physics mass scale. In Section 7 we compare the performance of $\sqrt{s}_{min}$ against some other inclusive variables which are commonly used in hadron collider physics for the purpose of estimating the new physics mass scale. Section 8 is reserved for our main summary and conclusions.

## 2. Definition of the RECO level variable $\sqrt{s}^{(reco)}_{min}$

In the first approach, we shall *not* modify the original definition of $\sqrt{s}_{min}$ and will continue to use the usual equation (1.2) (or its equivalent (1.4)), preserving the desired universal, global and inclusive character of the $\sqrt{s}_{min}$ variable. Then we shall concentrate on the question, how should one calculate the observable quantities $E$, $\vec{P}$ and $\not{P}_T$ entering the defining equations (1.2) and (1.4).

The previous $\sqrt{s}_{min}$ studies [1, 51, 52] used calorimeter-based measurements of the total visible energy $E$ and momentum $\vec{P}$ as follows. The total visible energy in the calorimeter $E_{(cal)}$ is simply a scalar sum over all calorimeter deposits

$$E_{(cal)} \equiv \sum_{\alpha} E_{\alpha} \ , \tag{2.1}$$

where the index $\alpha$ labels the calorimeter towers, and $E_{\alpha}$ is the energy deposit in the $\alpha$ tower. As usual, since muons do not deposit significantly in the calorimeters, the measured $E_{\alpha}$ should first be corrected for the energy of any muons which might be present in the event and happen to pass through the corresponding tower $\alpha$. The three components of the total

visible momentum $\vec{P}$ were also measured from the calorimeters as

$$P_{x(cal)} = \sum_{\alpha} E_\alpha \sin\theta_\alpha \cos\varphi_\alpha \ , \tag{2.2}$$

$$P_{y(cal)} = \sum_{\alpha} E_\alpha \sin\theta_\alpha \sin\varphi_\alpha \ , \tag{2.3}$$

$$P_{z(cal)} = \sum_{\alpha} E_\alpha \cos\theta_\alpha \ , \tag{2.4}$$

where $\theta_\alpha$ and $\varphi_\alpha$ are correspondingly the polar and azimuthal angular coordinates of the $\alpha$ calorimeter tower. The missing transverse momentum can similarly be measured from the calorimeter as (see eq. (1.6))

$$\vec{\not{P}}_{T(cal)} \equiv -\vec{P}_{T(cal)}. \tag{2.5}$$

Using these calorimeter-based measurements (2.1-2.5), one can make the identification

$$E \equiv E_{(cal)} \, , \tag{2.6}$$

$$\vec{P} \equiv \vec{P}_{(cal)} \, , \tag{2.7}$$

$$\vec{\not{P}}_T \equiv \vec{\not{P}}_{T(cal)} \tag{2.8}$$

in the definition (1.2) and construct the corresponding "calorimeter-based" $\sqrt{s}_{min}$ variable as

$$\sqrt{s}^{(cal)}_{min}(\not{M}) \equiv \sqrt{E^2_{(cal)} - P^2_{z(cal)}} + \sqrt{\not{M}^2 + \not{P}^2_{T(cal)}} \ . \tag{2.9}$$

This was precisely the quantity which was studied in [1, 51, 52] and shown to exhibit extreme sensitivity to the physics of the underlying event.

Here we propose to evaluate the visible quantities $E$ and $\vec{P}$ at the RECO level, i.e. in terms of the reconstructed objects, namely jets, muons, electrons and photons[4]. To be precise, let there be $N_{obj}$ reconstructed objects in the event, with energies $E_i$ and 3-momenta $\vec{P}_i$, $i = 1, 2, \ldots, N_{obj}$, correspondingly. Then in place of (2.6-2.8), let us instead identify

$$E \equiv E_{(reco)} \equiv \sum_{i=1}^{N_{obj}} E_i \, , \tag{2.10}$$

$$\vec{P} \equiv \vec{P}_{(reco)} \equiv \sum_{i=1}^{N_{obj}} \vec{P}_i \, , \tag{2.11}$$

$$\vec{\not{P}}_T \equiv \vec{\not{P}}_{T(reco)} = -\vec{P}_{T(reco)} \, , \tag{2.12}$$

and correspondingly define a "RECO-level" $\sqrt{s}_{min}$ variable as

$$\sqrt{s}^{(reco)}_{min}(\not{M}) \equiv \sqrt{E^2_{(reco)} - P^2_{z(reco)}} + \sqrt{\not{M}^2 + \not{P}^2_{T(reco)}} \ , \tag{2.13}$$

[4]This possibility was briefly alluded to in [1], but not pursued in any detail.

which can also be rewritten in analogy to (1.4) as

$$\sqrt{\hat{s}}_{min}^{(reco)}(\not{M}) \equiv \sqrt{M_{(reco)}^2 + P_{T(reco)}^2} + \sqrt{\not{M}^2 + \not{P}_{T(reco)}^2}\,, \tag{2.14}$$

where $\not{P}_{T(reco)}$ and $P_{T(reco)}$ are related as in eq. (2.12) and the RECO-level total visible mass $M_{(reco)}$ is defined by

$$M_{(reco)}^2 \equiv E_{(reco)}^2 - \vec{P}_{(reco)}^2\,. \tag{2.15}$$

What are the benefits from the new RECO-level $\sqrt{\hat{s}}_{min}$ definitions (2.13,2.14) in comparison to the old calorimeter-based $\sqrt{\hat{s}}_{min}$ definition in (2.9)? In order to understand the basic idea, it is worth comparing the calorimeter-based missing transverse momentum $\not{P}_T$ (which in the literature is commonly referred to as "missing transverse energy" $\not{E}_T$) and the analogous RECO-level variable $\not{H}_T$, the "missing $H_T$". The $\vec{\not{H}}_T$ vector is defined as the negative of the vector sum of the transverse momenta of all reconstructed objects in the event:

$$\vec{\not{H}}_T \equiv -\sum_{i=1}^{N_{obj}} \vec{P}_{Ti}\,. \tag{2.16}$$

Then it is clear that in terms of our notation here, $\not{H}_T$ is nothing but $\not{P}_{T(reco)}$.

It is known that $\not{H}_T$ performs better than $\not{E}_T$ [58]. First, $\not{H}_T$ is less affected by a number of adverse instrumental factors such as: electronic noise, faulty calorimeter cells, pile-up, etc. These effects tend to populate the calorimeter uniformly with unclustered energy, which will later fail the basic quality cuts during object reconstruction. In contrast, the *true* missing momentum is dominated by clustered energy, which will be successfully captured during reconstruction. Another advantage of $\not{H}_T$ is that one can easily apply the known jet energy corrections to account for the nonlinear detector response. For both of these reasons, CMS is now using $\not{H}_T$ at both the trigger level and offline [58].

Now realize that $\sqrt{\hat{s}}_{min}^{(cal)}$ is analogous to the calorimeter-based $\not{E}_T$, while our new variable $\sqrt{\hat{s}}_{min}^{(reco)}$ is analogous to the RECO-level $\not{H}_T$. Thus we may already expect that $\sqrt{\hat{s}}_{min}^{(reco)}$ will inherit the advantages of $\not{H}_T$ and will be better suited for determining the new physics mass scale than the calorimeter-based quantity $\sqrt{\hat{s}}_{min}^{(cal)}$. This expectation is confirmed in the explicit examples studied below in Secs. 4 and 5. Apart from the already mentioned instrumental issues, the most important advantage of $\sqrt{\hat{s}}_{min}^{(reco)}$ from the physics point of view is that it is much less sensitive to the effects from the underlying event, which had doomed its calorimeter-based $\sqrt{\hat{s}}_{min}^{(cal)}$ cousin.

Strictly speaking, the idea of $\sqrt{\hat{s}}_{min}^{(reco)}$ does not solve the underlying event problem completely and as a matter of principle. Every now and then the underlying event will still produce a well-defined jet, which will have to be included in the calculation of $\sqrt{\hat{s}}_{min}^{(reco)}$. Because of this effect, we cannot any more guarantee that $\sqrt{\hat{s}}_{min}^{(reco)}$ provides a lower bound on the true value $\sqrt{\hat{s}}_{true}$ of the center-of-mass energy of the hard scattering — the additional jets formed out of ISR, pile-up, and so on, will sometimes cause $\sqrt{\hat{s}}_{min}^{(reco)}$ to exceed $\sqrt{\hat{s}}_{true}$. Nevertheless we find that this effect modifies only the shape of the $\sqrt{\hat{s}}_{min}^{(reco)}$ distribution, but leaves the location of its peak largely intact. To the extent that one is mostly interested in the peak location, $\sqrt{\hat{s}}_{min}^{(reco)}$ should already be good enough for all practical purposes.

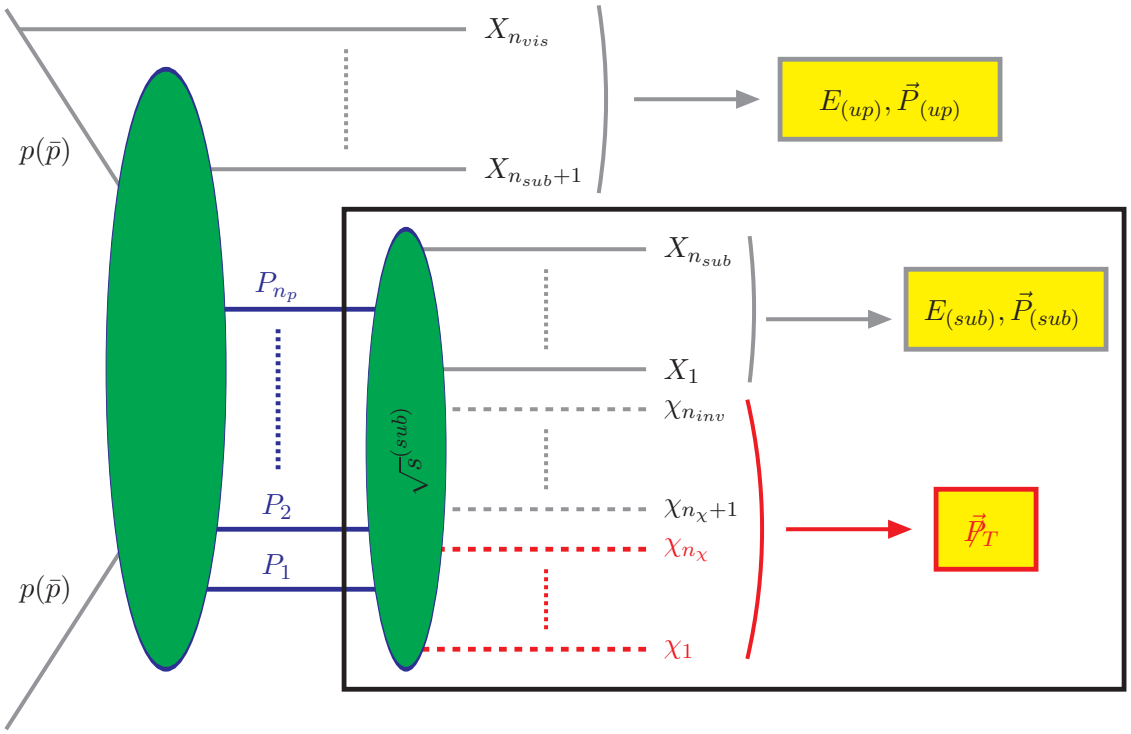


**Figure 2:** A rearrangement of Fig. 1 into an event topology exhibiting a well defined subsystem (delineated by the black rectangle) with total invariant mass $\sqrt{s}^{(sub)}$. There are $n_{sub}$ visible particles $X_i$, $i = 1, 2, \ldots, n_{sub}$, originating from within the subsystem, while the remaining $n_{vis} - n_{sub}$ visible particles $X_{n_{sub}+1}, \ldots, X_{n_{vis}}$ are created upstream, outside the subsystem. The subsystem results from the production and decays of a certain number of parent particles $P_j$, $j = 1, 2, \ldots, n_p$, (some of) which may decay semi-invisibly. All invisible particles $\chi_1, \ldots, \chi_{n_{inv}}$ are then assumed to originate from within the subsystem.

## 3. Definition of the subsystem variable $\sqrt{s}^{(sub)}_{min}$

In this section we propose an alternative modification of the original $\sqrt{s}_{min}$ variable, which solves the underlying event problem completely and as a matter of principle. The downside of this approach is that it is not as general and universal as the one discussed in the previous section, and can be applied only in cases where one can unambiguously identify a subsystem of the original event topology which is untouched by the underlying event. The basic idea is schematically illustrated in Fig. 2, which is nothing but a slight rearrangement of Fig. 1 exhibiting a well defined subsystem (delineated by the black rectangle). The original $n_{vis}$ visible particle $X_i$ from Fig. 1 have now been divided into two groups as follows:

1. There are $n_{sub}$ visible particles $X_1, \ldots, X_{n_{sub}}$ originating from within the subsystem. Their total energy and total momentum are denoted by $E_{(sub)}$ and $\vec{P}_{(sub)}$, correspond-

ingly. The subsystem particles are chosen so that to guarantee that they could not have come from the underlying event.

2. The remaining $n_{vis} - n_{sub}$ visible particles $X_{n_{sub}+1}, \ldots, X_{n_{vis}}$ are created upstream (outside the subsystem) and have total energy $E_{(up)}$ and total momentum $\vec{P}_{(up)}$. The upstream particles may originate from the underlying event or from decays of heavier particles upstream – this distinction is inconsequential at this point.

We also assume that all invisible particles $\chi_1, \ldots, \chi_{n_{inv}}$ originate from within the subsystem, i.e. that no invisible particles are created upstream. In effect, all we have done in Fig. 2 is to partition the original measured values of the total visible energy $E$ and 3-momentum $\vec{P}$ from Fig. 1 into two separate components as

$$E = E_{(up)} + E_{(sub)} \,, \tag{3.1}$$

$$\vec{P} = \vec{P}_{(up)} + \vec{P}_{(sub)} \,. \tag{3.2}$$

Notice that now the missing transverse momentum is defined as

$$\vec{\not{P}}_T \equiv -\vec{P}_{T(up)} - \vec{P}_{T(sub)} \,, \tag{3.3}$$

while the total visible invariant mass $M_{(sub)}$ of the subsystem is given by

$$M^2_{(sub)} = E^2_{(sub)} - \vec{P}^2_{(sub)} \,. \tag{3.4}$$

At this point the reader may be wondering what are the guiding principles for categorizing a given visible particle $X_i$ as a subsystem or an upstream particle. Since our goal is to identify a subsystem which is shielded from the effects of the underlying event, the safest way to do the partition of the visible particles is to require that all QCD jets belong to the upstream particles, while the subsystem particles consist of objects which are unlikely to come from the underlying event, such as isolated electrons, photons and muons (and possibly identified $\tau$-jets and, to a lesser extent, tagged $b$-jets).

With those preliminaries, we are now ready to ask the usual $\sqrt{s}_{min}$ question: Given the measured values of $E_{(up)}$, $E_{(sub)}$, $\vec{P}_{(up)}$ and $\vec{P}_{(sub)}$, what is the minimum value $\sqrt{s}^{(sub)}_{min}$ of the *subsystem* Mandelstam invariant mass variable $\sqrt{s}^{(sub)}$, which is consistent with those measurements? Proceeding as in [1], once again we find a very simple universal answer, which, with the help of (3.3) and (3.4), can be equivalently written in several different ways

as follows:

$$\sqrt{s}_{min}^{(sub)}(\not{M}) = \left\{ \left( \sqrt{E_{(sub)}^2 - P_{z(sub)}^2} + \sqrt{\not{M}^2 + \not{P}_T^2} \right)^2 - P_{T(up)}^2 \right\}^{\frac{1}{2}} \tag{3.5}$$

$$= \left\{ \left( \sqrt{M_{(sub)}^2 + P_{T(sub)}^2} + \sqrt{\not{M}^2 + \not{P}_T^2} \right)^2 - P_{T(up)}^2 \right\}^{\frac{1}{2}} \tag{3.6}$$

$$= \left\{ \left( \sqrt{M_{(sub)}^2 + P_{T(sub)}^2} + \sqrt{\not{M}^2 + \not{P}_T^2} \right)^2 - (\vec{P}_{T(sub)} + \vec{\not{P}}_T)^2 \right\}^{\frac{1}{2}} \tag{3.7}$$

$$= ||p_{T(sub)} + \not{p}_T|| \,, \tag{3.8}$$

where in the last line we have introduced the Lorentz 1+2 vectors

$$p_{T(sub)} \equiv \left( \sqrt{M_{(sub)}^2 + P_{T(sub)}^2} \,,\, \vec{P}_{T(sub)} \right) ; \tag{3.9}$$

$$\not{p}_T \equiv \left( \sqrt{\not{M}^2 + \not{P}_T^2} \,,\, \vec{\not{P}}_T \right) . \tag{3.10}$$

As usual, the length of a 1+2 vector is computed as $||p|| = \sqrt{p \cdot p} = \sqrt{p_0^2 - p_1^2 - p_2^2}$.

Before we proceed to the examples of the next few sections, as a sanity check of the obtained result it is useful to consider some limiting cases. First, by taking the upstream visible particles to be an empty set, i.e. $\vec{P}_{T(up)} \to 0$, we recover the usual expression for $\sqrt{s}_{min}$ given in eqs. (1.2,1.4). Next, consider a case with no invisible particles, i.e. $\not{M} = 0$ and correspondingly, $\vec{\not{P}}_T = 0$. In that case we obtain that $\sqrt{s}_{min}^{(sub)} = M_{(sub)}$, which is of course the correct result. Finally, suppose that there are no visible subsystem particles, i.e. $E_{(sub)} = \vec{P}_{(sub)} = M_{(sub)} = 0$. In that case we obtain $\sqrt{s}_{min}^{(sub)} = \not{M}$, which is also the correct answer.

As we shall see, the subsystem concept of Fig. 2 will be most useful when the subsystem results from the production and decays of a certain number $n_p$ of parent particles $P_j$ with masses $M_{P_j}$, $j = 1, 2, \ldots, n_p$, correspondingly. Then the total combined mass of all parent particles is given by

$$M_p \equiv \sum_{j=1}^{n_p} M_{P_j} \,. \tag{3.11}$$

By the conjecture of ref. [1], the location of the peak of the $\sqrt{s}_{min}^{(sub)}(\not{M})$ distribution will provide an approximate measurement of $M_p$ as a function of the unknown parameter $\not{M}$. By construction, the obtained relationship $M_p(\not{M})$ will then be completely insensitive to the effects from the underlying event.

At this point it may seem that by excluding all QCD jets from the subsystem, we have significantly narrowed down the number of potential applications of the $\sqrt{s}_{min}^{(sub)}$ variable. Furthermore, we have apparently reintroduced a certain amount of model-dependence which the original $\sqrt{s}_{min}$ approach was trying so hard to avoid. Those are in principle valid objections,

which can be overcome by using the $\sqrt{\hat{s}}_{min}^{(reco)}$ variable introduced in the previous section. Nevertheless, we feel that the $\sqrt{\hat{s}}_{min}^{(sub)}$ variable can prove to be useful in its own right, and in a wide variety of contexts. To see this, note that the typical hadron collider signatures of the most popular new physics models (supersymmetry, extra dimensions, Little Higgs, etc.) are precisely of the form exhibited in Fig. 2. One typically considers production of colored particles (squarks, gluinos, KK-quarks, etc.) whose cross-sections dominate. In turn, these colored particles shed their color charge by emitting jets and decaying to lighter, uncolored particles in an electroweak sector. The decays of the latter often involve electromagnetic objects, which could be targeted for selection in the subsystem. The $\sqrt{\hat{s}}_{min}^{(sub)}$ variable would then be the perfect tool for studying the mass scales in the electroweak sector (in the context of supersymmetry, for example, the electroweak sector is composed of the charginos, neutralinos and sleptons).

Before we move on to some specific examples illustrating these ideas, one last comment is in order. One may wonder whether the $\sqrt{\hat{s}}_{min}^{(sub)}$ variable should be computed at the RECO-level or from the calorimeter. Since the subsystem will usually be defined in terms of reconstructed objects, the more logical option is to calculate $\sqrt{\hat{s}}_{min}^{(sub)}$ at the RECO-level and label it as $\sqrt{\hat{s}}_{min}^{(sub,reco)}$. However, to streamline our notation, in what follows we shall always omit the "reco" part of the superscript and will always implicitly assume that $\sqrt{\hat{s}}_{min}^{(sub)}$ is computed at RECO-level.

## 4. SM example: dilepton events from $t\bar{t}$ production

In this and the next two sections we illustrate the properties of the new variables $\sqrt{\hat{s}}_{min}^{(reco)}$ and $\sqrt{\hat{s}}_{min}^{(sub)}$ with some specific examples. In this section we discuss an example taken from the Standard Model, which is guaranteed to be available for early studies at the LHC. We consider dilepton events from $t\bar{t}$ pair production, where both $W$'s decay leptonically. In this event topology, there are two missing particles (two neutrinos). Therefore, these events very closely resemble the typical SUSY-like events, in which there are two missing dark matter particles. In the next two sections, we shall also consider some SUSY examples. In all cases, we perform detailed event simulation, including the effects from the underlying event and detector resolution.

### 4.1 Event simulation details

Events are generated with PYTHIA [59] (using its default model of the underlying event) at an LHC of 14 TeV, and then reconstructed with the PGS detector simulation package [60]. We have made certain modifications in the publicly available version of PGS to better match it to the CMS detector. For example, we take the hadronic calorimeter resolution to be [61]

$$\frac{\sigma}{E} = \frac{120\%}{\sqrt{E}}\,, \tag{4.1}$$

while the electromagnetic calorimeter resolution is [61]

$$\left(\frac{\sigma}{E}\right)^2 = \left(\frac{S}{\sqrt{E}}\right)^2 + \left(\frac{N}{E}\right)^2 + C^2\,, \tag{4.2}$$

where the energy $E$ is measured in GeV, $S = 3.63\%$ is the stochastic term, $N = 0.124$ is the noise and $C = 0.26\%$ is the constant term. Muons are reconstructed within $|\eta| < 2.4$, and we use the muon global reconstruction efficiency quoted in [61]. We use default $p_T$ cuts on the reconstructed objects as follows: 3 GeV for muons, 10 GeV for electrons and photons, and 15 GeV for jets.

For the $t\bar{t}$ example presented in this section, we use the approximate next-to-next-to-leading order $t\bar{t}$ cross-section of $\sigma_{t\bar{t}} = 894 \pm 4^{+73+12}_{-46-12}$ pb at a top mass of $m_t = 175$ GeV [62]. For the SUSY examples in the next two sections we use leading order cross-sections.

Since our examples are meant for illustration purposes only, we do not include any backgrounds to the processes being considered, nor do we require any specific triggers. A detailed study of the dilepton $t\bar{t}$ signature including all those effects will appear elsewhere [63].

### 4.2 $\sqrt{s}^{(reco)}_{min}$ variable

We first consider SUSY-like missing energy events arising from $t\bar{t}$ production, where each $W$-boson is forced to decay leptonically (to an electron or a muon). We do not impose any trigger or offline requirements, and simply plot directly the output from PGS[5]. We show various $\sqrt{s}$ quantities of interest in Fig. 3, setting $\not{M} = 0$, since in this case the missing particles are neutrinos and are massless. The dotted (yellow-shaded) histogram represents the true $\sqrt{s}$ distribution of the $t\bar{t}$ pair. It quickly rises at the $t\bar{t}$ mass threshold

$$M_p \equiv 2m_t = 350 \text{ GeV} \tag{4.3}$$

and then eventually falls off at large $\sqrt{s}$ due to the parton density function suppression. Because the top quarks are typically produced with some boost, the $\sqrt{s}_{true}$ distribution in Fig. 3 peaks a little bit above threshold:

$$\left(\sqrt{s}_{true}\right)_{peak} > M_p\,. \tag{4.4}$$

It is clear that if one could directly measure the $\sqrt{s}_{true}$ distribution, or at least its onset, the $t\bar{t}$ mass scale will be easily revealed. Unfortunately, the escaping neutrinos make such a measurement impossible, unless one is willing to make additional model-dependent assumptions[6].

[5]Therefore, our plots in this subsection are normalized to a total number of events equal to $\sigma_{t\bar{t}} \times BR(W \to e, \mu)^2$.

[6]For example, one can use the known values of the neutrino, $W$ and top masses to solve for the neutrino kinematics (up to discrete ambiguities). However, this method assumes that the full mass spectrum is already known, and furthermore, uses the knowledge of the top decay topology to perfectly solve the combinatorics problem discussed in the Introduction. As an example, consider a case where the lepton is produced first and the $b$-quark second, i.e. when the top first decays to a lepton and a leptoquark, which in turn decays to a neutrino and a $b$-quark. The kinematic method would then be using the wrong on-shell conditions. The advantage of the $\sqrt{s}_{min}$ approach is that it is fully inclusive and does not make any reference to the actual decay topology.

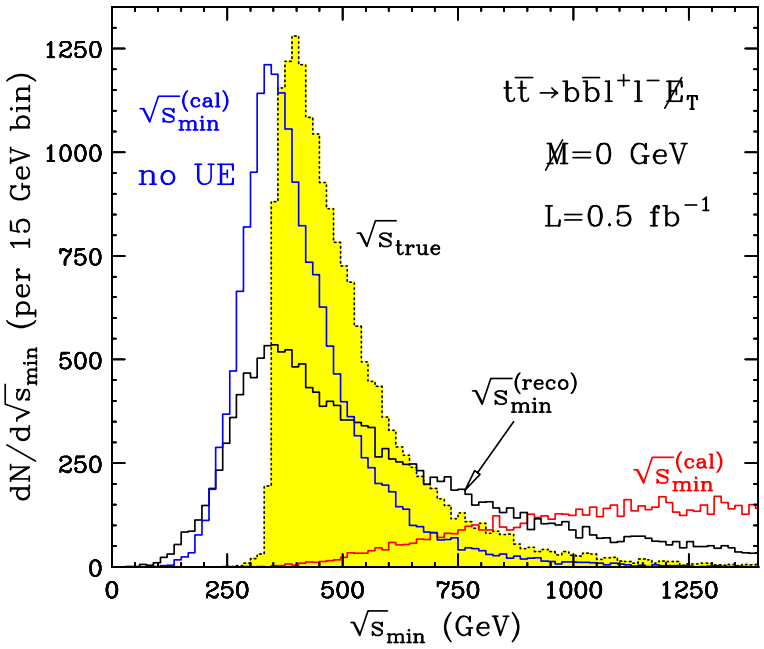


**Figure 3:** Distributions of various $\sqrt{s}_{min}$ quantities discussed in the text, for the dilepton $t\bar{t}$ sample at the LHC with 14 TeV CM energy and 0.5 fb$^{-1}$ of data. The dotted (yellow-shaded) histogram gives the true $\sqrt{s}$ distribution of the $t\bar{t}$ pair. The blue histogram is the distribution of the calorimeter-based $\sqrt{s}_{min}^{(cal)}$ variable in the ideal case when all effects from the underlying event are turned off. The red histogram shows the corresponding result for $\sqrt{s}_{min}^{(cal)}$ in the presence of the underlying event. The black histogram is the distribution of the $\sqrt{s}_{min}^{(reco)}$ variable introduced in Sec. 2. All $\sqrt{s}_{min}$ distributions are shown for $\not{M} = 0$.

Fig. 3 also shows two versions of the calorimeter-based $\sqrt{s}_{min}^{(cal)}$ variable: the blue (red) histogram is obtained by switching off (on) the underlying event (ISR and MPI). These curves reveal two very interesting phenomena. First, without the UE, the peak of the $\sqrt{s}_{min}^{(cal)}$ distribution (blue histogram) is very close to the parent mass threshold [1]:

$$\text{no UE} \implies \left(\sqrt{s}_{min}^{(cal)}\right)_{peak} \approx M_p\,. \tag{4.5}$$

The main observation of Ref. [1] was that this correlation offers an alternative, fully inclusive and model-independent, method of estimating the mass scale $M_p$ of the parent particles, even when some of their decay products are invisible and not seen in the detector.

Unfortunately, the "no UE" limit of eq. (4.5) is unphysical, and the corresponding $\sqrt{s}_{min}^{(cal)}$ distribution (blue histogram in in Fig. 3) is unobservable. What is worse, when one tries to measure the $\sqrt{s}_{min}^{(cal)}$ distribution in the presence of the UE (red histogram in Fig. 3), the resulting peak is very far from the physical threshold:

$$\text{with UE} \implies \left(\sqrt{s}_{min}^{(cal)}\right)_{peak} \gg M_p\,. \tag{4.6}$$

In the $t\bar{t}$ example of Fig. 3, the shift is on the order of 1 TeV! It appears therefore that in practice the $\sqrt{s}_{min}^{(cal)}$ peak would be uncorrelated with any physical mass scale, and instead would be completely determined by the (uninteresting) physics of the underlying event. Once the nice model-independent correlation of eq. (4.5) is destroyed by the UE, it becomes of only academic value [1, 6, 51–53].

However, Fig. 3 also suggests the solution to this difficult problem. If we look at the distribution of the $\sqrt{s}_{min}^{(reco)}$ variable (black solid histogram), we see that its peak has returned to the desired value:

$$\left(\sqrt{s}_{min}^{(reco)}\right)_{peak} \approx M_p \,, \tag{4.7}$$

thus resurrecting the original proposal of Ref. [1]. In order to measure physical mass thresholds, one simply needs to investigate the distribution of the inclusive $\sqrt{s}_{min}^{(reco)}$ variable, which is calculated at RECO-level. Each peak in that distribution signals the opening of a new channel, and from (4.7) the location of the peak provides an immediate estimate of the total mass of all particles involved in the production. Of course, the $\sqrt{s}_{min}^{(reco)}$ distribution is now not as sharply peaked as the unphysical "no UE" case of $\sqrt{s}_{min}^{(cal)}$, but as long as its peak is found in the right location, the method of Ref. [1] becomes viable once again.

Our first main result is therefore nicely summarized in Fig. 3, which shows a total of 4 distributions, 3 of which are either unphysical (the blue histogram of $\sqrt{s}_{min}^{(cal)}$ *in the absence* of the UE), unobservable (the yellow-shaded histogram of $\sqrt{s}_{true}$), or useless (the red histogram of $\sqrt{s}_{min}^{(cal)}$ *in the presence* of the UE). The only distribution in Fig. 3 which is physical, observable and useful at the same time, is the distribution of $\sqrt{s}_{min}^{(reco)}$ (solid black histogram).

Before concluding this subsection, we explain the reason for the improved performance of the $\sqrt{s}_{min}^{(reco)}$ variable in comparison to the $\sqrt{s}_{min}^{(cal)}$ version. As already anticipated in Sec. 2, the basic idea is that energy deposits which are due to hard particles originating from the hard scattering, tend to be clustered, while the energy deposits due to the UE tend to be more uniformly spread throughout the detector. In order to see this pictorially, in Figs. 4 and 5 we show a series of calorimeter maps of the combined ECAL+HCAL energy deposits as a function of the pseudorapidity $\eta$ and azimuthal angle $\phi$. Since the calorimeter in PGS is segmented in cells of $(\Delta\eta, \Delta\phi) = (0.1, 0.1)$, each calorimeter tower is represented by a square pixel, which is color-coded according to the amount of energy present in the tower. We have chosen the color scheme so that larger deposits correspond to darker colors.

Each calorimeter map figure below has four panels. In the upper two panels the calorimeter is filled at the parton level directly from PYTHIA. This corresponds to a perfect detector, where we ignore any smearing effects due to the finite energy resolution. The lower two plots in each figure show the corresponding results after PGS simulation. Thus by comparing the plots in the upper row to those in the bottom row, one can see the effect of the detector resolution. While the finite detector resolution does play some role, we find that it is of no particular importance for understanding the reason behind the big swings in the $\sqrt{s}_{min}$ peaks observed in Fig. 3.

Let us instead concentrate on comparing the plots in the left column versus those in the right column. The left plots show the absolute energy deposit $E_\alpha$ in the $\alpha$ calorimeter

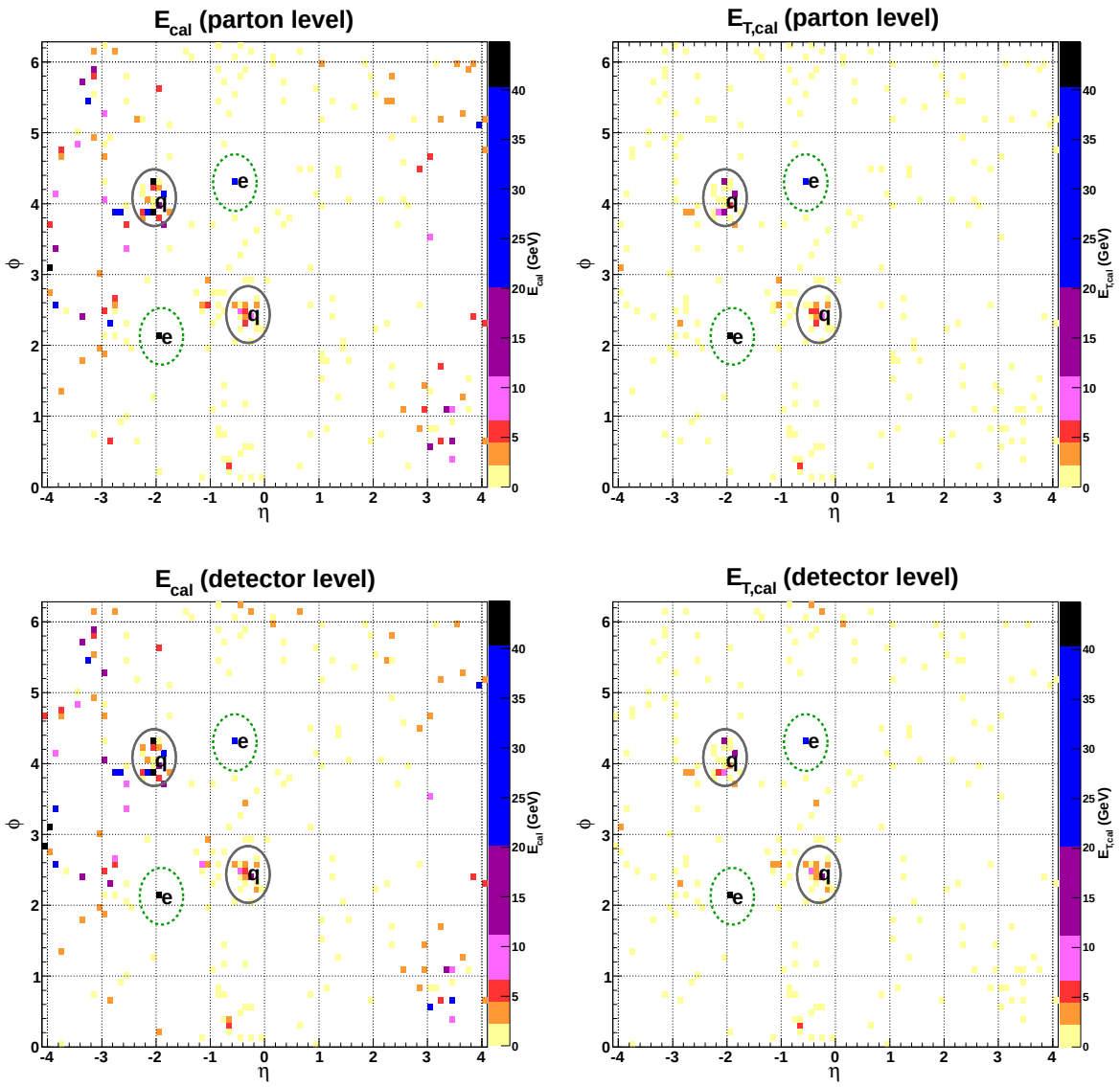


**Figure 4:** PGS calorimeter map of the energy deposits, as a function of pseudorapidity $\eta$ and azimuthal angle $\phi$, for a dilepton $t\bar{t}$ event with only two reconstructed jets. At the parton level, this particular event has two $b$-quarks and two electrons. The location of a $b$-quark (electron, muon) is marked with the letter "q" ("e", "$\mu$"). A grey circle delineates (the cone of) a reconstructed jet, while a green dotted circle denotes a reconstructed lepton. In the upper two plots the calorimeter is filled at the parton level directly from PYTHIA, while the lower two plots contain results after PGS simulation. The left plots show absolute energy deposits $E_\alpha$, while in the right plots the energy in each tower is shown projected on the transverse plane as $E_\alpha \cos\theta_\alpha$.

tower, while in the right plots this energy is shown projected on the transverse plane as $E_\alpha \cos\theta_\alpha$. The difference between the left and the right plots is quite striking. The plots

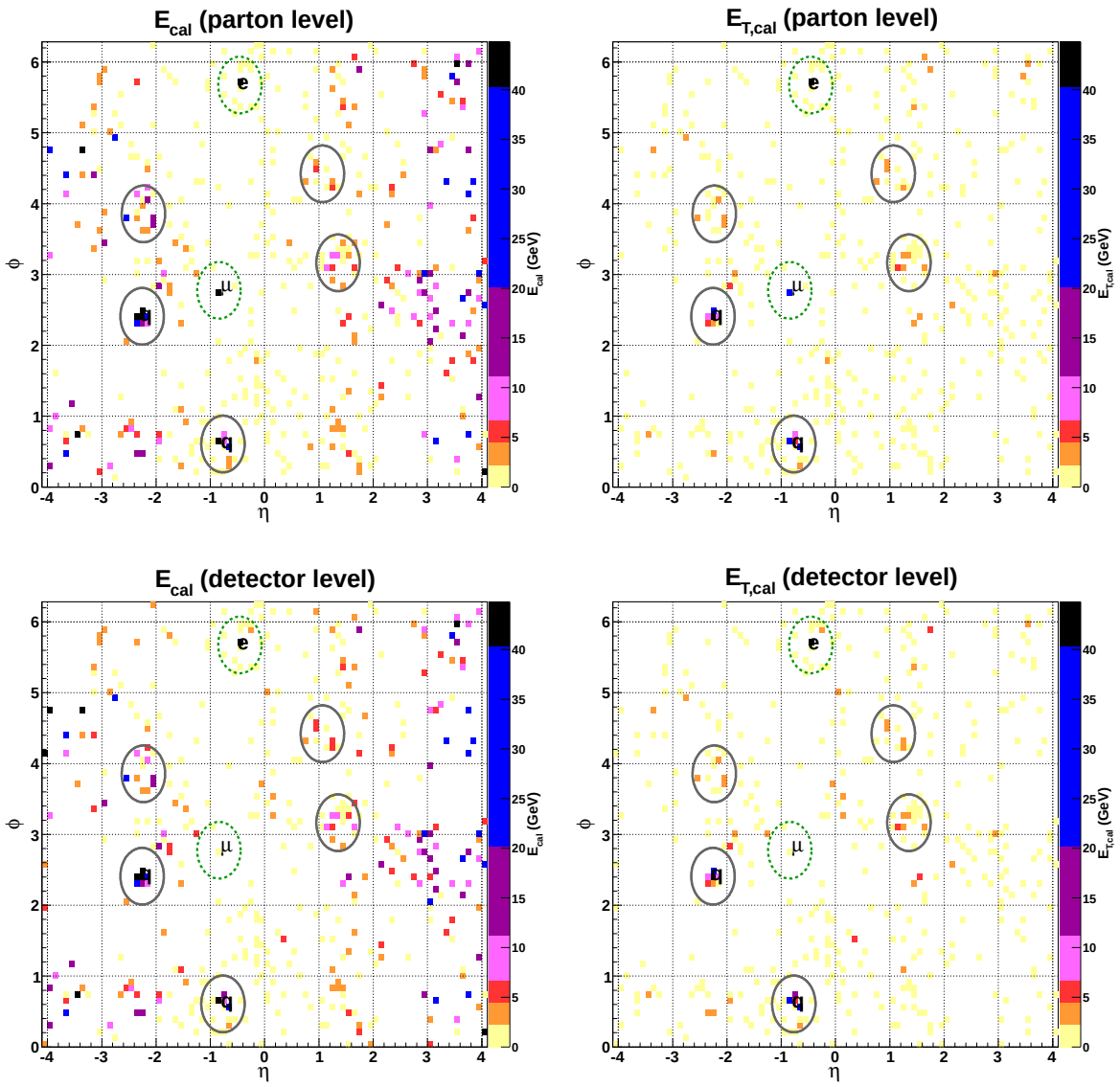


**Figure 5:** The same as Fig. 4, but for an event with three additional reconstructed jets.

on the left exhibit lots of energy, which is deposited mostly in the forward calorimeter cells (at large $|\eta|$) [1]. The plots on the right, on the other hand, show only a few clusters of energy, concentrated mostly in the central part of the detector. Those energy clusters give rise to the objects (jets, electrons and photons) which are reconstructed from the calorimeter. Furthermore, each energy cluster can be easily identified with a parton-level particle in the top decay chain. In order to exhibit this correlation, in Figs. 4 and 5 we use the following notation for the parton-level particles: a $b$-quark (electron, muon) is marked with the letter "q" ("e", "$\mu$"). A grey circle delineates (the cone of) a reconstructed jet, while a green dotted circle

| Event type | PYTHIA parton level | | after PGS simulation | |
|---|---|---|---|---|
| | $\sqrt{s}_{true}$ | $\sqrt{s}^{(cal)}_{min}$ | $\sqrt{s}^{(cal)}_{min}$ | $\sqrt{s}^{(reco)}_{min}$ |
| $t\bar{t}$ event in Fig. 4 | 427 | 1110 | 1179 | 363 |
| $t\bar{t}$ event in Fig. 5 | 638 | 2596 | 2761 | 736 |
| SUSY event in Fig. 12 | 1954 | 3539 | 3509 | 2085 |

**Table 1:** Selected $\sqrt{s}$ quantities (in GeV) for the events shown in Figs. 4, 5 and 12. The second column shows the true invariant mass $\sqrt{s}_{true}$ of the parent system: top quark pair in case of Figs. 4 and 5, or gluino pair in case of Fig. 12. The third column shows the value of the $\sqrt{s}^{(cal)}_{min}$ variable (2.9) calculated at the parton level, without any PGS detector simulation, but with the full detector acceptance cut of $|\eta| < 4.1$. The fourth column lists the value of $\sqrt{s}^{(cal)}_{min}$ obtained after PGS detector simulation, while the last column shows the value of the $\sqrt{s}^{(reco)}_{min}$ variable defined in (2.13).

marks a reconstructed lepton (electron or muon). The lepton isolation requirement implies that green circles should be void of large energy deposits off-center, and indeed we observe this to be the case.

In particular, Fig. 4 shows a bare-bone dilepton $t\bar{t}$ event with just two reconstructed jets and two reconstructed leptons (which happen to be both electrons). As seen in the figure, the two jets can be easily traced back to the two $b$-quarks at the parton level, and there are no additional reconstructed jets due to the UE activity. Because the event is so clean and simple, one might expect to obtain a reasonable value for $\sqrt{s}_{min}$, i.e. close to the $t\bar{t}$ threshold. However, this is not the case, if we use the calorimeter-based measurement $\sqrt{s}^{(cal)}_{min}$. As seen in Table 1, the measured value of $\sqrt{s}^{(cal)}_{min}$ is very far off — on the order of 1 TeV, even in the case of a perfect detector. The reason for this discrepancy is now easy to understand from Fig. 4. Recall that $\sqrt{s}^{(cal)}_{min}$ is defined in terms of the *total* energy $E_{(cal)}$ in the calorimeter, which in turn is dominated by the large deposits in the forward region, which came from the underlying event. More importantly, those contributions are more or less equally spread over the forward and backward region of the detector, leading to cancellations in the calculation of the corresponding longitudinal $P_{z(cal)}$ momentum component. As a result, the first term in (2.9) becomes completely dominated by the UE contributions [51].

Let us now see how the calculation of $\sqrt{s}^{(reco)}_{min}$ is affected by the UE. Since object reconstruction is done with the help of minimum *transverse* cuts (for clustering and object id), the relevant calorimeter plots are the maps on the right side in Fig. 4. We see that the large forward energy deposits which were causing the large shift in $\sqrt{s}^{(cal)}_{min}$ are not incorporated into any reconstructed objects, and thus do not contribute to the $\sqrt{s}^{(reco)}_{min}$ calculation at all. In effect, the RECO-level prescription for calculating $\sqrt{s}_{min}$ is leaving out precisely the unwanted contributions from the UE, while keeping the relevant contributions from the hard scattering. As seen from Table 1, the calculated value of $\sqrt{s}^{(reco)}_{min}$ for that event is 363 GeV, which is indeed very close to the $t\bar{t}$ threshold. It is also smaller than the true $\sqrt{s}$ value of 427 GeV in that event, which is to be expected, since by design $\sqrt{s}_{min} \leq \sqrt{s}$, and this event does not have any extra ISR jets to spoil this relation.

It is instructive to consider another, more complex $t\bar{t}$ dilepton event, such as the one

shown in Fig. 5. The corresponding calculated values for $\sqrt{s}_{min}^{(cal)}$ and $\sqrt{s}_{min}^{(reco)}$ are shown in the second row of Table 1. As seen in Fig. 5, this event has additional jets and a lot more UE activity. As a result, the calculated value of $\sqrt{s}_{min}^{(cal)}$ is shifted by almost 2 TeV from the nominal $\sqrt{s}_{true}$ value. Nevertheless, the RECO-level prescription nicely compensates for this effect, and the calculated $\sqrt{s}_{min}^{(reco)}$ value is only 736 GeV, which is within 100 GeV of the nominal $\sqrt{s}_{true} = 638$ GeV. Notice that in this example we end up with a situation where $\sqrt{s}_{min}^{(reco)} > \sqrt{s}_{true}$. Fig. 3 indicates that this happens quite often — the tail of the $\sqrt{s}_{min}^{(reco)}$ distribution is more populated than the (yellow-shaded) $\sqrt{s}_{true}$ distribution. This should be no cause for concern. First of all, we are only interested in the *peak* of the $\sqrt{s}_{min}^{(reco)}$ distribution, and we do not need to make any comparisons between $\sqrt{s}_{min}^{(reco)}$ and $\sqrt{s}_{true}$. Second, any such comparison would be meaningless, since the value of $\sqrt{s}_{true}$ is a priori unknown, and unobservable.

### 4.3 $\sqrt{s}_{min}^{(sub)}$ variable

Before concluding this section, we shall use the $t\bar{t}$ example to also illustrate the idea of the subsystem $\sqrt{s}_{min}^{(sub)}$ variable developed in Sec. 3. Dilepton $t\bar{t}$ events are a perfect testing ground for this idea, since the $WW$ subsystem decays leptonically, without any jet activity. We therefore define the subsystem as the two hard isolated leptons resulting from the decays of the $W$-bosons. Correspondingly, we require two reconstructed leptons (electrons or muons) at the PGS level[7], and plot the distribution of the leptonic subsystem $\sqrt{s}_{min}^{(sub)}$ variable in Fig. 6. As before, the dotted (yellow-shaded) histogram represents the true $\sqrt{s}$ distribution of the $W^+W^-$ pair. As expected, it quickly rises at the $WW$ threshold (denoted by the vertical arrow), then falls off at large $\sqrt{s}$. Since the $\sqrt{s}_{true}^{(WW)}$ distribution is unobservable, the best we can do is to study the corresponding $\sqrt{s}_{min}^{(sub)}$ distribution shown with the solid black histogram. In this subsystem example, all UE activity is lumped together with the upstream $b$-jets from the top quarks decays, and thus has no bearing on the properties of the leptonic $\sqrt{s}_{min}^{(sub)}$. In particular, we find that the value of $\sqrt{s}_{min}^{(sub)}$ is always smaller than the true $\sqrt{s}_{true}^{(WW)}$. More importantly, Fig. 6 demonstrates that the peak in the $\sqrt{s}_{min}^{(sub)}$ distribution is found precisely at the mass threshold of the particles (in this case the two $W$ bosons) which initiated the subsystem. Therefore, in analogy to (4.7) we can also write

$$\left(\sqrt{s}_{min}^{(sub)}\right)_{peak} \approx M_p^{(sub)}\,, \tag{4.8}$$

where $M_p^{(sub)}$ is the combined mass of all the parents initiating the subsystem. Fig. 6 shows that in the $t\bar{t}$ example just considered, this relation holds to a very high degree of accuracy.

This example should not leave the reader with the impression that hadronic jets are never allowed to be part of the subsystem. On the contrary — the subsystem may very well include reconstructed jets as well. The $t\bar{t}$ case considered here in fact provides a perfect example to illustrate the idea.

[7]The selection efficiency for the two leptons is on the order of 60%, which explains the different normalization of the distributions in Figs. 3 and 6.

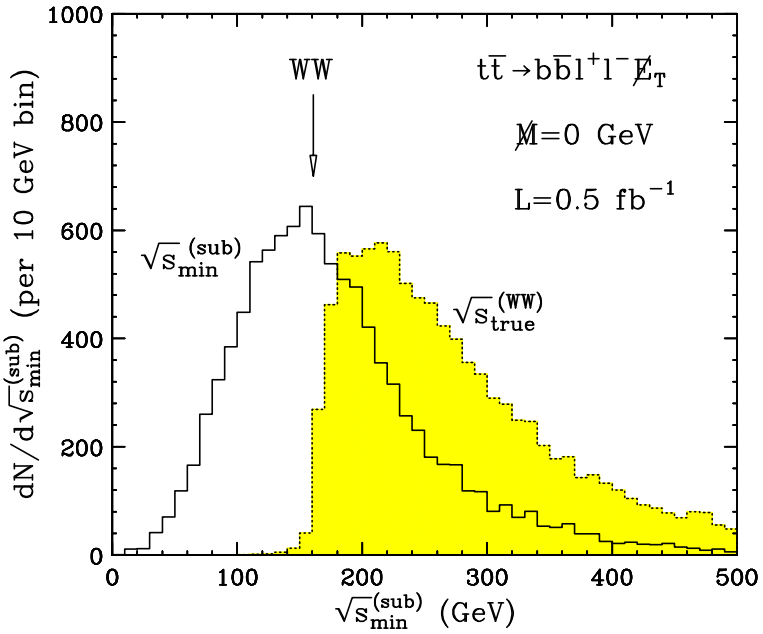


**Figure 6:** The same as Fig. 3, but for the dilepton subsystem in dilepton $t\bar{t}$ events with two reconstructed leptons in PGS. The dotted (yellow-shaded) histogram gives the true $\sqrt{s}$ distribution of the $W^+W^-$ pair in those events. The black histogram shows the distribution of the (leptonic) subsystem variable $\sqrt{s}_{min}^{(sub)}$ defined in Sec. 3. In this case, the subsystem is defined by the two isolated leptons, while all jets are treated as upstream particles. The vertical arrow marks the $W^+W^-$ mass threshold.

Let us reconsider the $t\bar{t}$ dilepton sample, and redefine the subsystem so that we now target the two *top quarks* as the parents initiating the subsystem. Correspondingly, in addition to the two leptons, let us allow the subsystem to include two jets, presumably coming from the two top quark decays. Unfortunately, in doing so, we must face a variant of the partitioning[8] combinatorial problem discussed in the introduction: as seen in Fig. 7, the typical jet multiplicity in the events is relatively high, and we must therefore specify the exact procedure how to select the two jets which would enter the subsystem. We shall consider three different approaches.

- *B-tagging.* We can use the fact that the jets from top quark decay are $b$-jets, while the jets from ISR are typically light flavor jets. Therefore, by requiring exactly two $b$-tags, and including only the two $b$-tagged jets as part of the subsystem, we can significantly increase the probability of selecting the correct jets. Of course, ISR will sometimes also contribute $b$-tagged jets from gluon splitting, but that happens rather rarely and the corresponding contribution can be suppressed by a further invariant mass cut on the two $b$-jets. The resulting $\sqrt{s}_{min}^{(sub)}$ distribution for the subsystem of 2 leptons and 2 $b$-tagged jets is shown in Fig. 8 with the black histogram. We see that, as expected, the distribution peaks at the $t\bar{t}$ threshold and this time provides a measurement of the

[8]By construction, the $\sqrt{s}_{min}$ and $\sqrt{s}_{min}^{(sub)}$ variables never have to face the *ordering* combinatorial problem.

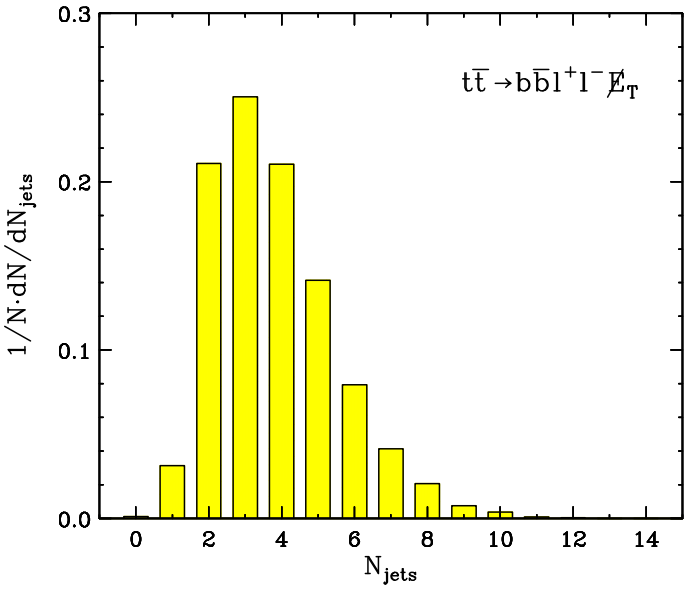


**Figure 7:** Unit-normalized distribution of jet multiplicity in dilepton $t\bar{t}$ events.

top quark mass:

$$\left(\sqrt{s}_{min}^{(sub)}\right)_{peak} \approx M_p^{(sub)} = 2m_t = 350 \text{ GeV}\,. \tag{4.9}$$

The disadvantage of this method is the loss in statistics: compare the normalization of the black histogram in Fig. 8 after applying the two $b$-tags, to the dotted (yellow-shaded) distribution of the true $t\bar{t}$ distribution in the selected inclusive dilepton sample (without $b$-tags).

- *Selection by jet $p_T$.* Here one can use the fact that the jets from top decays are on average harder than the jets from ISR. Correspondingly, by choosing the two highest $p_T$ jets (regardless of $b$-tagging), one also increases the probability to select the correct jet pair. The corresponding distribution is shown in Fig. 8 with the blue histogram, and is also seen to peak at the $t\bar{t}$ threshold. An important advantage of this method is that one does not have to pay the price of reduced statistics due to the two additional $b$-tags.

- *No selection.* The most conservative approach would be to apply no selection criteria on the jets, and include all reconstructed jets in the subsystem. Then the subsystem $\sqrt{s}_{min}^{(sub)}$ variable essentially reverts back to the RECO-level inclusive variable $\sqrt{s}_{min}^{(reco)}$ already discussed in the previous subsection. Not surprisingly, we find the peak of its distribution (red histogram in Fig. 8) near the $t\bar{t}$ threshold as well.

All three of these examples show that jets can also be usefully incorporated into the subsystem. The only question is whether one can find a reliable way of preferentially selecting jets which are more likely to originate from within the intended subsystem, as opposed to

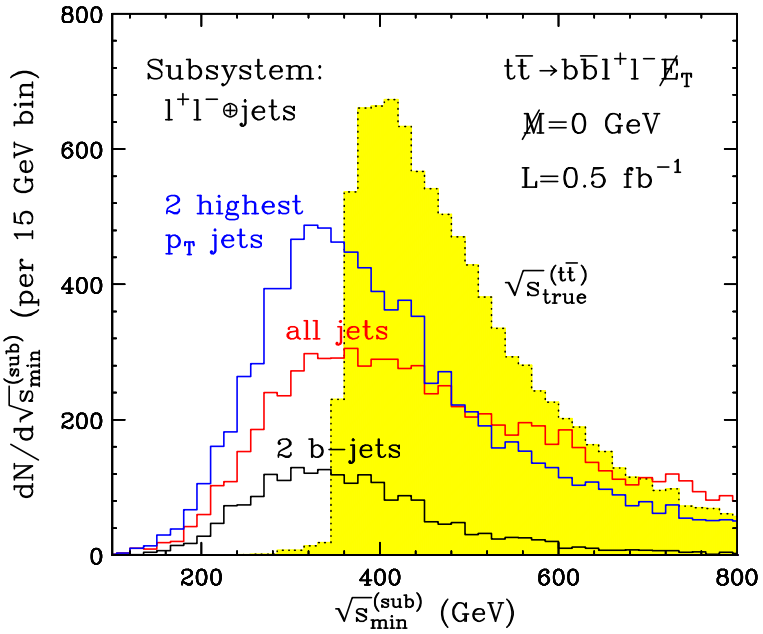


**Figure 8:** The same as Fig. 6, but in addition to the two leptons, the subsystem now also includes: exactly two $b$-tagged jets (black histogram); the two highest $p_T$ jets (blue histogram); or all jets (red histogram). The dotted (yellow-shaded) histogram gives the true $\sqrt{s}$ distribution of the $t\bar{t}$ pair.

from the outside. As we see in Fig. 8, in the $t\bar{t}$ case this is quite possible, although in general it may be difficult in other settings, like the SUSY examples discussed in the next section.

## 5. An exclusive SUSY example: multijet events from gluino production

Since $\sqrt{s}_{min}$ is a fully inclusive variable, arguably its biggest advantage is that it can be applied to purely jetty events with large jet multiplicities, where no other method on the market would seem to work. In order to simulate such a challenging case, we consider gluino pair production in supersymmetry, with each gluino forced to undergo a cascade decay chain involving only QCD jets and nothing else. For concreteness, we revisit the setup of Ref. [1], where two different possibilities for the gluino decays were considered:

- In one scenario, the gluino $\tilde{g}$ is forced to undergo a two-stage cascade decay to the LSP. In the first stage, the gluino decays to the second-lightest neutralino $\tilde{\chi}^0_2$ and two quark jets: $\tilde{g} \to q\bar{q}\tilde{\chi}^0_2$. In turn, $\tilde{\chi}^0_2$ itself is then forced to decay via a 3-body decay to 2 quark jets and the LSP: $\tilde{\chi}^0_2 \to q\bar{q}\tilde{\chi}^0_1$. The resulting gluino signature is 4 jets plus missing energy:

$$\tilde{g} \to jj\tilde{\chi}^0_2 \to jjjj\tilde{\chi}^0_1 \ . \tag{5.1}$$

  Therefore, gluino pair production will nominally result in 8 jet events. Of course, as shown in Fig. 9, the actual number of reconstructed jets in such events is even higher, due to the effects of ISR, FSR and/or string fragmentation. As seen from the figure, each

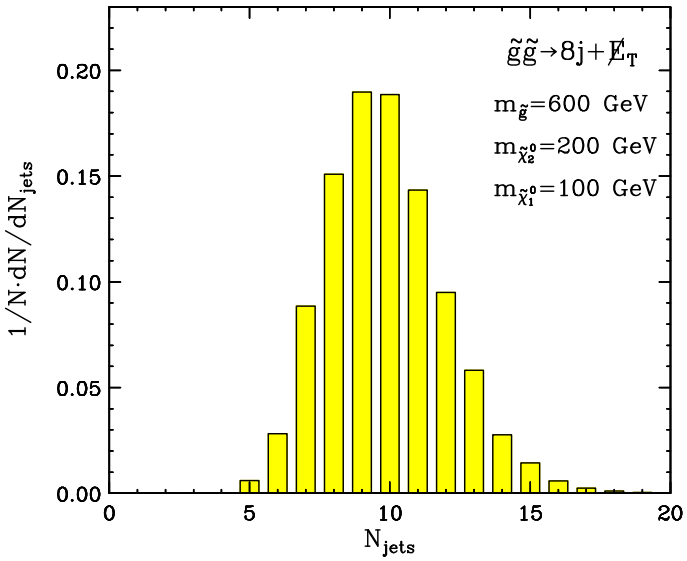


**Figure 9:** Unit-normalized distribution of jet multiplicity in gluino pair production events, with each gluino decaying to four jets and a $\tilde{\chi}_1^0$ LSP as in (5.1).

such event has on average $\sim 10$ jets, presenting a formidable combinatorics problem. We suspect that all[9] mass reconstruction methods on the market are doomed if they were to face such a scenario. It is therefore of particular interest to see how well the $\sqrt{s}_{min}$ method (which is advertized as universally applicable) would fare under such dire circumstances.

- In the second scenario, the gluino decays directly to the LSP via a three-body decay

$$\tilde{g} \to jj\tilde{\chi}_1^0 \ , \tag{5.2}$$

so that gluino pair-production events would nominally have 4 jets and missing energy.

For concreteness, in each scenario we fix the mass spectrum as was done in [1]: we use the approximate gaugino unification relations to relate the gaugino and neutralino masses as

$$m_{\tilde{g}} = 3m_{\tilde{\chi}_2^0} = 6m_{\tilde{\chi}_1^0} \ . \tag{5.3}$$

We can then vary one of these masses, and choose the other two in accord with these relations. Since we assume three-body decays in (5.2) and (5.1), we do not need to specify the SUSY scalar mass parameters, which can be taken to be very large. In addition, as implied by (5.3), we imagine that the lightest two neutralinos are gaugino-like, so that we do not have to specify the higgsino mass parameter either, and it can be taken to be very large as well.

After these preliminaries, our results for these two scenarios are shown in Figs. 10 and 11, correspondingly. In Fig. 10 (Fig. 11) we consider the 8-jet signature arising from (5.1)

[9]With the possible exception of the $M_{Tgen}$ method of Ref. [32], see Section 7 below.

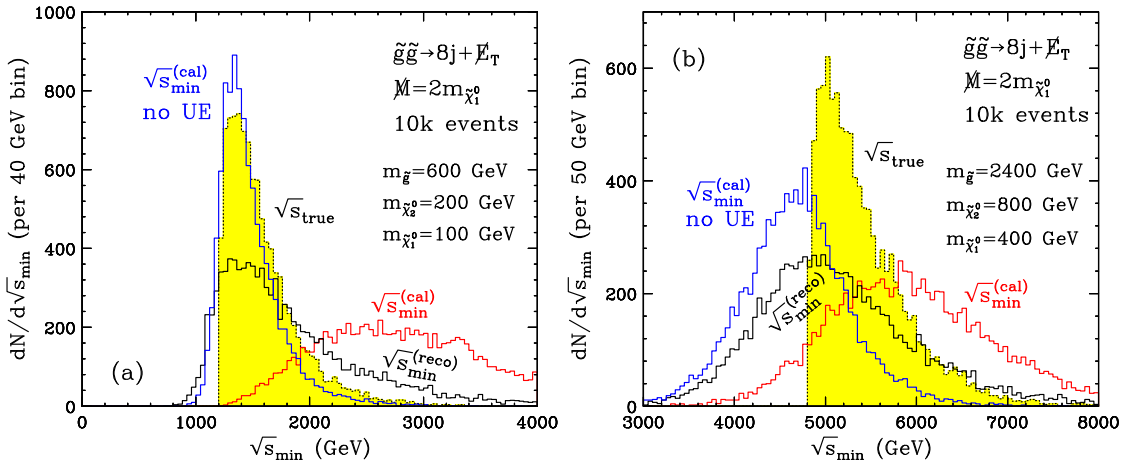


**Figure 10:** The same as Fig. 3, but for a SUSY example of gluino pair production, with each gluino decaying to four jets and a $\tilde{\chi}_1^0$ LSP as indicated in (5.1). The mass spectrum is chosen as: (a) $m_{\tilde{g}} = 600$ GeV, $m_{\tilde{\chi}_2^0} = 200$ GeV and $m_{\tilde{\chi}_1^0} = 100$ GeV; or (b) $m_{\tilde{g}} = 2400$ GeV, $m_{\tilde{\chi}_2^0} = 800$ GeV and $m_{\tilde{\chi}_1^0} = 400$ GeV. All three $\sqrt{s}_{min}$ distributions are plotted for the correct value of the missing mass parameter, in this case $\not{M} = 2m_{\tilde{\chi}_1^0}$.

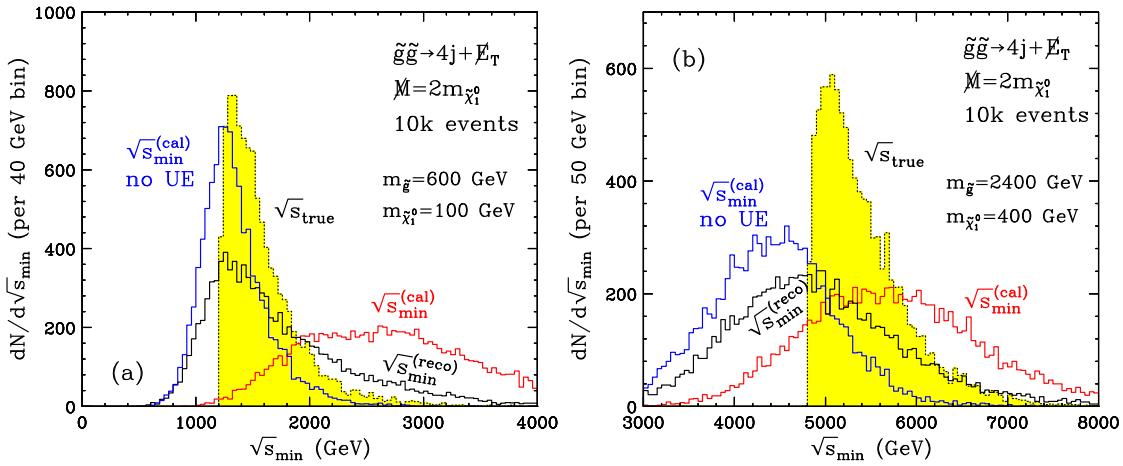


**Figure 11:** The same as Fig. 10, but for the case of gluino decays to 2 jets and a $\tilde{\chi}_1^0$ LSP as in (5.2).

(the 4-jet signature arising from (5.2)). In both figures, panels (a) correspond to a light mass spectrum $m_{\tilde{g}} = 600$ GeV, $m_{\tilde{\chi}_2^0} = 200$ GeV and $m_{\tilde{\chi}_1^0} = 100$ GeV; while panels (b) correspond to a heavy mass spectrum $m_{\tilde{g}} = 2400$ GeV, $m_{\tilde{\chi}_2^0} = 800$ GeV and $m_{\tilde{\chi}_1^0} = 400$ GeV. Each plot shows the same four distributions as in Fig. 3. The $\sqrt{s}_{min}$ distributions are all plotted for the correct value of the missing mass parameter, namely $\not{M} = 2m_{\tilde{\chi}_1^0}$.

Overall, the results seen in Figs. 10 and 11 are not too different from what we already witnessed in Fig. 3 for the $t\bar{t}$ example. The (unobservable) distribution $\sqrt{s}_{true}$ shown with the dotted yellow-shaded histogram has a sharp turn-on at the physical mass threshold $M_p =$

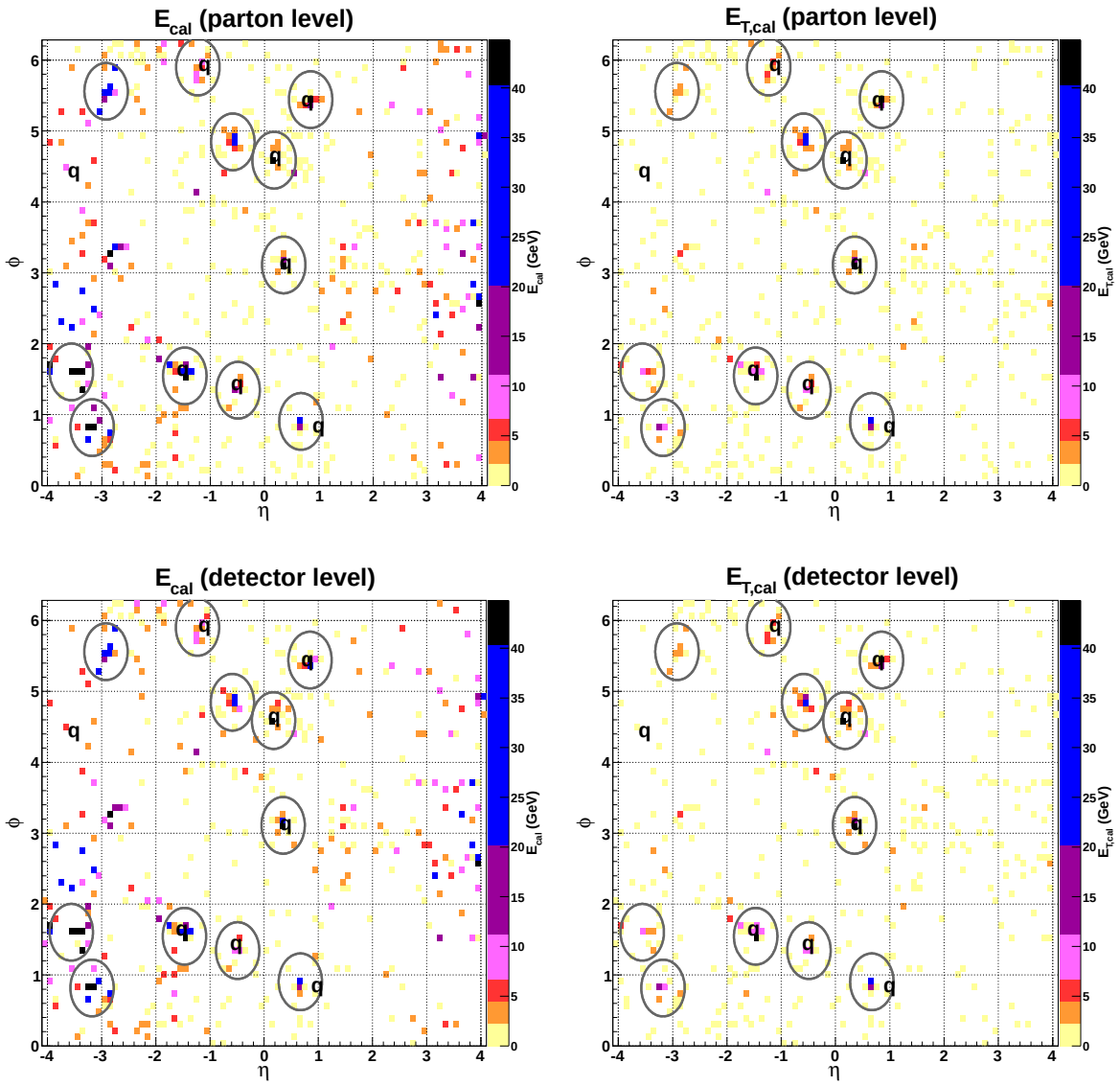


**Figure 12:** The same as Fig. 4, but for a SUSY event of gluino pair production, with each gluino forced to decay to 4 jets and the LSP as in (5.1). The SUSY mass spectrum is as in Figs. 10(a) and 11(a): $m_{\tilde{g}} = 600$ GeV, $m_{\tilde{\chi}_2^0} = 200$ GeV and $m_{\tilde{\chi}_1^0} = 100$ GeV. As in Figs. 4 and 5, the circles denote jets reconstructed in PGS, and here "q" marks the location of a quark from a gluino decay chain. Therefore, a circle without a "q" inside corresponds to a jet resulting from ISR or FSR, while a letter "q" without an accompanying circle represents a quark in the gluino decay chain which was not subsequently reconstructed as a jet.

$2m_{\tilde{g}}$. If the effects of the UE are ignored, the position of this threshold is given rather well by the peak of the $\sqrt{\hat{s}}_{min}^{(cal)}$ distribution (blue histogram). Unfortunately, the UE shifts the peak in $\sqrt{\hat{s}}_{min}^{(cal)}$ by 1-2 TeV (red histogram). Fortunately, the distribution of the RECO-level

variable $\sqrt{s}_{min}^{(reco)}$ (black histogram) is stable against UE contamination, and its peak is still in the right place (near $M_p$).

Having already seen a similar behavior in the $t\bar{t}$ example of the previous section, these results may not seem very impressive, until one realizes just how complicated those events are. For illustration, Fig. 12 shows the previously discussed calorimeter maps for one particular "8 jet" event. This event happens to have 11 reconstructed jets, which is consistent with the typical jet multiplicity seen in Fig. 9. The values of the $\sqrt{s}$ quantities of interest for this event are listed in Table 1. We see that the RECO prescription for calculating $\sqrt{s}_{min}$ is able to compensate for a shift in $\sqrt{s}$ of more than 1.5 TeV! A casual look at Fig. 12 should be enough to convince the reader just how daunting the task of mass reconstruction in such events is. In this sense, the ease with which the $\sqrt{s}_{min}$ method reveals the gluino mass scale in Figs. 10 and 11 is quite impressive.

## 6. An inclusive SUSY example: GMSB study point GM1b

In the Introduction we already mentioned that $\sqrt{s}_{min}$ is a fully inclusive variable. Here we would like to point out that there are two different aspects of the inclusivity property of $\sqrt{s}_{min}$:

- *Object-wise inclusivity:* $\sqrt{s}_{min}$ is inclusive with regards to the type of reconstructed objects. The definition of $\sqrt{s}_{min}^{(reco)}$ does not distinguish between the different types of reconstructed objects (and $\sqrt{s}_{min}^{(cal)}$ makes no reference to any reconstructed objects at all). This makes $\sqrt{s}_{min}$ a very convenient variable to use in those cases where the newly produced particles have many possible decay modes, and restricting oneself to a single exclusive signature would cause loss in statistics. For illustration, consider the gluino pair production example from the previous section. Even though we are always producing the same type of parent particles (two gluinos), in general they can have several different decay modes, leading to a very diverse sample of events with varying number of jets and leptons. Nevertheless, the $\sqrt{s}_{min}^{(reco)}$ distribution, plotted over this whole signal sample, will still be able to pinpoint the gluino mass scale, as explained in Sec. 5.

- *Event-wise inclusivity:* $\sqrt{s}_{min}$ is inclusive also with regards to the type of events, i.e. the type of new particle production. For simplicity, in our previous examples we have been considering only one production mechanism at a time, but this is not really necessary — $\sqrt{s}_{min}$ can also be applied in the case of several simultaneous production mechanisms.

In order to illustrate the last point, in this section we shall consider the simultaneous production of the full spectrum of SUSY particles at a particular benchmark point. We chose the GM1b CMS study point [64], which is nothing but a minimal gauge-mediated SUSY-breaking (GMSB) scenario on the SPS8 Snowmass slope [65]. The input parameters are $\Lambda$=80 TeV, $M_{mes}$=160 TeV, $N_{mes}$=1, $\tan\beta = 15$ and $\mu > 0$. The physical mass spectrum is given in Table 2. Point GM1b is characterized by a neutralino NLSP, which promptly decays

| $\tilde{u}_L$ | $\tilde{d}_L$ | $\tilde{u}_R$ | $\tilde{d}_R$ | $\tilde{\ell}_L$ | $\tilde{\nu}_\ell$ | $\tilde{\ell}_R$ | $\tilde{\chi}_2^\pm$ | $\tilde{\chi}_4^0$ | $\tilde{\chi}_3^0$ | $\tilde{g}$ |
|---|---|---|---|---|---|---|---|---|---|---|
| 908 | 911 | 872 | 870 | 289 | 278 | 145 | 371 | 371 | 348 | 690 |
| $\tilde{t}_1$ | $\tilde{b}_1$ | $\tilde{t}_2$ | $\tilde{b}_2$ | $\tilde{\tau}_2$ | $\tilde{\nu}_\tau$ | $\tilde{\tau}_1$ | $\tilde{\chi}_1^\pm$ | $\tilde{\chi}_2^0$ | $\tilde{\chi}_1^0$ | $\tilde{G}$ |
| 806 | 863 | 895 | 878 | 290 | 277 | 138 | 206 | 206 | 106 | 0 |

**Table 2:** Masses (in GeV) of the SUSY particles at the GM1b study point. Here $\tilde{u}$ and $\tilde{d}$ ($\tilde{\ell}$ and $\tilde{\nu}_\ell$) stand for either of the first two generations squarks (sleptons).

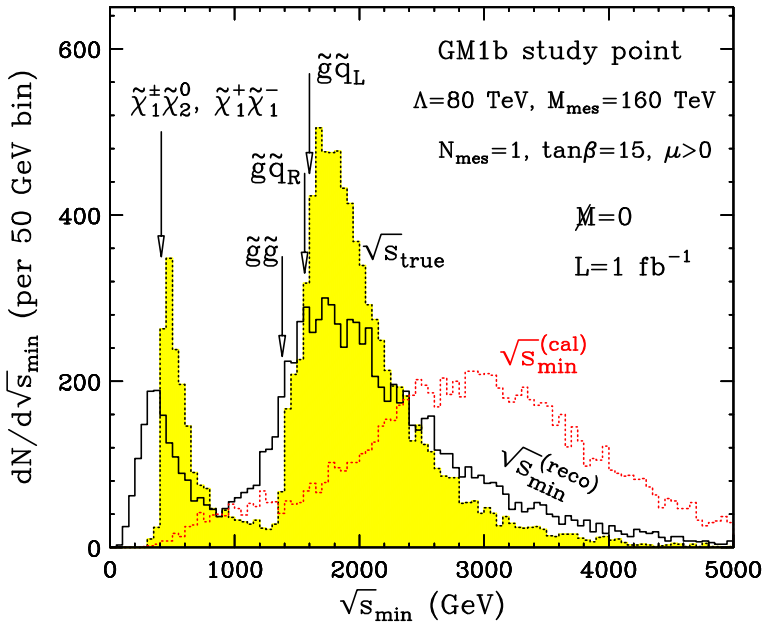


**Figure 13:** Distribution of the $\sqrt{s}_{min}^{(cal)}$ (dotted red) and $\sqrt{s}_{min}^{(reco)}$ (solid black) variables in inclusive SUSY production for the GMSB GM1a benchmark study point with parameters $\Lambda = 80$ TeV, $M_{mes} = 160$ TeV, $N_{mes} = 1$, $\tan\beta = 15$ and $\mu > 0$. The dotted yellow-shaded histogram is the true $\sqrt{s}$ distribution of the parent pair of SUSY particles produced at the top of each decay chain (the identity of the parent particles varies from event to event). The $\sqrt{s}_{min}$ distributions are shown for $\not{M} = 0$ and are normalized to 1 fb$^{-1}$ of data. The vertical arrows mark the mass thresholds for a few dominant SUSY pair-production processes.

(predominantly) to a photon and a gravitino. Therefore, a typical event has two hard photons and missing energy, which provide good handles for suppressing the SM backgrounds.

We now consider inclusive production of all SUSY subprocesses and plot the $\sqrt{s}_{min}$ distributions of interest in Fig. 13. As usual, the dotted yellow-shaded histogram is the true $\sqrt{s}$ distribution of the parent pair of SUSY particles produced at the top of each decay chain. Since we do not fix the production subprocess, the identity of the parent particles varies from event to event. Naturally, the most common parent particles are the ones with the highest production cross-sections. For point GM1b, at a 14 TeV LHC, strong SUSY production dominates, and is 87% of the total cross-section. A few of the dominant subprocesses and their cross-sections are listed in Table 3.

| Process | $\tilde{\chi}_1^\pm\tilde{\chi}_2^0$ | $\tilde{\chi}_1^+\tilde{\chi}_1^-$ | $\tilde{g}\tilde{g}$ | $\tilde{g}\tilde{q}_R$ | $\tilde{g}\tilde{q}_L$ | $\tilde{q}_R\tilde{q}_R$ | $\tilde{q}_L\tilde{q}_R$ | $\tilde{q}_L\tilde{q}_L$ |
|---|---|---|---|---|---|---|---|---|
| $\sigma$ (pb) | 0.83 | 0.43 | 2.03 | 2.17 | 1.90 | 0.36 | 0.50 | 0.28 |
| $M_p$ (GeV) | 412 | 412 | 1380 | $\sim 1560$ | $\sim 1600$ | $\sim 1740$ | $\sim 1780$ | $\sim 1820$ |

**Table 3:** Cross-sections (in pb) and parent mass thresholds (in GeV) for the dominant production processes at the GM1b study point. The listed squark cross-sections are summed over the light squark flavors and conjugate states. The total SUSY cross-section at point GM1b is 9.4 pb.

The true $\sqrt{s}$ distribution in Fig. 13 exhibits an interesting double-peak structure, which is easy to understand as follows. As we have seen in the exclusive examples from Secs. 4 and 5, at hadron colliders the particles tend to be produced with $\sqrt{s}$ close to their mass threshold. As seen in Table 2, the particle spectrum of the GM1b point can be broadly divided (according to mass) into two groups of superpartners: electroweak sector (the lightest chargino $\tilde{\chi}_1^\pm$, second-to-lightest neutralino $\tilde{\chi}_2^0$ and sleptons) with a mass scale on the order of 200 GeV and a strong sector (squarks and gluino) with masses of order $700-900$ GeV. The first peak in the true $\sqrt{s}$ distribution (near $\sqrt{s} \sim 500$ GeV) arises from the pair production of two particles from the electroweak sector, while the second, broader peak in the range of $\sqrt{s} \sim 1500-2300$ GeV is due to the pair production of two colored superpartners[10]. Each one of those peaks is made up of several contributions from different individual subprocesses, but because their mass thresholds[11] are so close, in the figure they cannot be individually resolved, and appear as a single bump.

If one could somehow directly observe the true $\sqrt{s}$ SUSY distribution (the dotted yellow-shaded histogram in Fig. 13), this would lead to some very interesting conclusions. First, from the presence of two separate peaks one would know immediately that there are two widely separated scales in the problem. Second, the normalization of each peak would indicate the relative size of the total inclusive cross-sections (in this example, of the particles in the electroweak sector versus those in the strong sector). Finally, the broadness of each peak is indicative of the total number of contributing subprocesses, as well as the typical mass splittings of the particles within each sector. It may appear surprising that one is able to draw so many conclusions from a single distribution of an inclusive variable, but this just comes to show the importance of $\sqrt{s}$ as one of the fundamental collider physics variables.

Unfortunately, because of the missing energy due to the escaping invisible particles, the true $\sqrt{s}$ distribution cannot be observed, and the best one can do to approximate it is to look at the distributions of our inclusive $\sqrt{s}_{min}$ variables discussed in Sec. 2: the calorimeter-based $\sqrt{s}_{min}^{(cal)}$ variable (dotted red histogram in Fig. 13) and the RECO-level $\sqrt{s}_{min}^{(reco)}$ variable (solid black histogram in Fig. 13). In the figure, both of those are plotted for $\not{M} = 0$.

First let us concentrate on the calorimeter-based version $\sqrt{s}_{min}^{(cal)}$ (dotted red histogram). We can immediately see the detrimental effects of the UE: first, the electroweak production peak has been almost completely smeared out, while the strong production peak has been

[10]The attentive reader may also notice two barely visible bumps (near 950 GeV and 1150 GeV) reflecting the associated production of one colored and one uncolored particle: $\tilde{g}\tilde{\chi}_1^\pm, \tilde{g}\tilde{\chi}_2^0$ and $\tilde{q}\tilde{\chi}_1^\pm, \tilde{q}\tilde{\chi}_2^0$, correspondingly.

[11]A few individual mass thresholds are indicated by vertical arrows in Fig. 13.

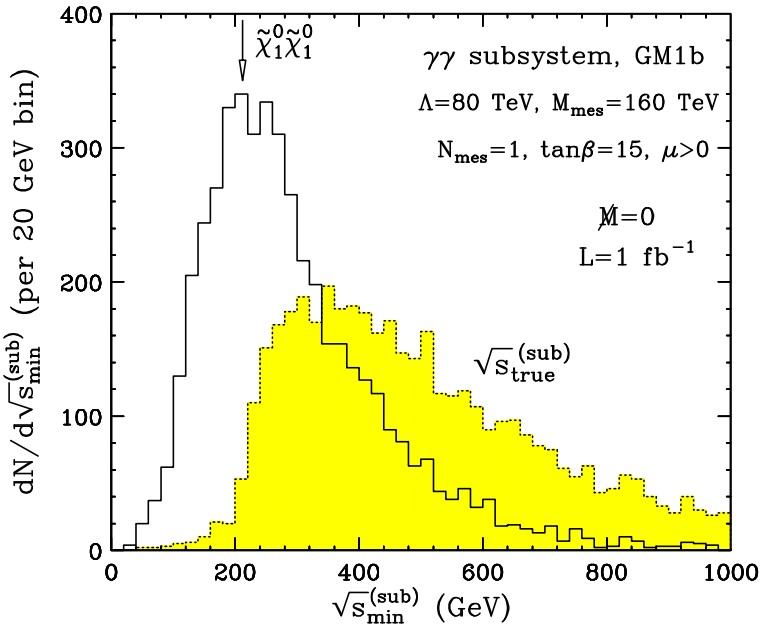


**Figure 14:** The same as Fig. 6, but for the GMSB SUSY example considered in Fig. 13. Here the subsystem is defined in terms of the two hard photons resulting from the two $\tilde{\chi}_1^0 \to \tilde{G} + \gamma$ decays. The vertical arrow marks the onset for inclusive $\tilde{\chi}_1^0\tilde{\chi}_1^0$ production.

shifted upwards by more than a TeV! This behavior is not too surprising, since the same effect was already encountered in our previous examples in Secs. 4 and 5. Fortunately, we now also know the solution to this problem: one needs to consider the RECO-level variable $\sqrt{s}_{min}^{(reco)}$ instead, which tracks the true $\sqrt{s}$ distribution much better. We can see evidence of this in Fig. 13 as well: notice how the (black) $\sqrt{s}_{min}^{(reco)}$ histogram exhibits the same features as the (yellow-shaded) true $\sqrt{s}$ distribution. In particular, $\sqrt{s}_{min}^{(reco)}$ does show two separate peaks (indicating that SUSY production takes place at two different mass scales), the peaks are in their proper locations (relative to the missing mass scale $\not{M}$), and have the correct relative width, hinting at the size of the mass splittings in each sector. We thus conclude that all of the interesting physics conclusions that one would be able to reach from looking at the true $\sqrt{s}$ distributions, can still be made based on the inclusive distribution of our RECO-level $\sqrt{s}_{min}^{(reco)}$ variable.

Before concluding this section, we shall take the opportunity to use the GM1b example to also illustrate the $\sqrt{s}_{min}^{(sub)}$ variable proposed in Sec. 3. As already mentioned, the GM1b study point corresponds to a GMSB scenario with a promptly decaying Bino-like $\tilde{\chi}_1^0$ NLSP. Most events therefore contain two hard photons from the two $\tilde{\chi}_1^0$ decays to gravitinos. Then it is quite natural to define the exclusive subsystem in Fig. 2 in terms of these two photons. The corresponding $\sqrt{s}_{min}^{(sub)}$ distribution is shown in Fig. 14 with the black solid histogram. For completeness, in the figure we also show the true $\sqrt{s}$ distribution of the $\tilde{\chi}_1^0$ pair (dotted yellow-shaded histogram). The vertical arrow marks the location of the $\tilde{\chi}_1^0\tilde{\chi}_1^0$ mass threshold.

We notice that the peak of the $\sqrt{s}_{min}^{(sub)}$ distribution nicely reveals the location of the neutralino mass threshold, and from there the neutralino mass itself. We see that the method of $\sqrt{s}_{min}^{(sub)}$ provides a very simple way of measuring the NLSP mass in such GMSB scenarios (for an alternative approach based on $M_{T2}$, see [66]).

## 7. Comparison to other inclusive collider variables

Having discussed the newly proposed variables $\sqrt{s}_{min}^{(reco)}$ and $\sqrt{s}_{min}^{(sub)}$ in various settings in Secs. 4-6, we shall now compare them to some other global inclusive variables which have been discussed in the literature in relation to determining a mass scale of the new physics. For simplicity here we shall concentrate only on the most model-independent variables, which do not suffer from the topological and combinatorial ambiguities mentioned in the Introduction.

At the moment, there are only a handful of such variables. Depending on the treatment of the unknown masses of the invisible particles, they can be classified into one of the following two categories:

- *Variables which do not depend on an unknown invisible mass parameter.* The most popular members of this class are the "missing $H_T$" variable

$$\not{H}_T \equiv \left| -\sum_{i=1}^{N_{obj}} \vec{P}_{Ti} \right| , \tag{7.1}$$

  which is simply the magnitude of the $\vec{\not{H}}_T$ vector from eq. (2.16), and the scalar $H_T$ variable

$$H_T \equiv \not{H}_T + \sum_{i=1}^{N_{obj}} P_{Ti} \, . \tag{7.2}$$

  Here we follow the notation from Sec. 2, where $\vec{P}_{Ti}$ is the measured transverse momentum of the $i$-th reconstructed object in the event ($i = 1, 2, \ldots, N_{obj}$). The main advantage of $\not{H}_T$ and $H_T$ is their simplicity: both are very general, and are defined purely in terms of observed quantities, without any unknown mass parameters. The downside of $\not{H}_T$ and $H_T$ is that they cannot be directly correlated with any physical mass scale in a model-independent way[12].

- *Variables which exhibit dependence on one or more invisible mass parameters.* As two representatives from this class we shall consider $M_{Tgen}$ from Ref. [32] and $\sqrt{s}_{min}^{(reco)}$ from Sec. 2 here. We shall not repeat the technical definition of $M_{Tgen}$, and instead refer the uninitiated reader to the original paper [32]. Suffice it to say that the method of $M_{Tgen}$ starts out by assuming exactly two decay chains in each event. The arising combinatorial problem is then solved by brute force — by considering all possible partitions of the

[12]Some early studies of $H_T$-like variables found interesting linear correlations between the peak in the $H_T$ distribution and a suitably defined SUSY mass scale in the context of specific SUSY models, e.g. minimal supergravity (MSUGRA) [10,67,68], minimal GMSB [67], or mixed moduli-mediation [69]. However, any such correlations do not survive further scrutiny in more generic SUSY scenarios, see e.g. [70].

event into two sides, computing $M_{T2}$ for each such partition, and taking the minimum value of $M_{T2}$ found in the process. Both $M_{Tgen}$ and $\sqrt{\hat{s}}_{min}^{(reco)}$ introduce a priori unknown parameters related to the mass scale of the missing particles produced in the event. In the case of $\sqrt{\hat{s}}_{min}^{(reco)}$, this is simply the single parameter $\not{M}$, measuring the *total* invisible mass (in the sense of a scalar sum as defined in eq. (1.3)). The $M_{Tgen}$ variable, on the other hand, must in principle introduce two separate missing mass parameters $\not{M}_1$ and $\not{M}_2$ (one for each side of the event). However, the existing applications of $M_{Tgen}$ in the literature have typically made the assumption that $\not{M}_1 = \not{M}_2$, although this is not really necessary and one could just as easily work in terms of two separate inputs $\not{M}_1$ and $\not{M}_2$ [3, 4]. The inconvenience of having to deal with unknown mass parameters in the case of $M_{Tgen}$ and $\sqrt{\hat{s}}_{min}^{(reco)}$ is greatly compensated by the luxury of being able to relate certain features of their distributions to a fundamental physical mass scale in a robust, model-independent way. In particular, the upper *endpoint* $M_{Tgen}^{(max)}$ of the $M_{Tgen}$ distribution gives the larger of the two parent masses $\max\{M_{P_1}, M_{P_2}\}$ [71]. Therefore, if the two parent masses are the same, i.e. $M_{P_1} = M_{P_2}$, then the parent mass threshold $M_p = M_{P_1} + M_{P_2}$ is simply given by

$$M_p = 2M_{Tgen}^{(max)}. \tag{7.3}$$

On the other hand, as we have already seen in Secs. 4-6, the *peak* of the $\sqrt{\hat{s}}_{min}^{(reco)}$ is similarly correlated with the parent mass threshold, see eq. (4.7).

In principle, all four[13] of these variables are inclusive both object-wise and event-wise. It is therefore of interest to compare them with respect to:

1. The degree of correlation with the new physics mass scale $M_p$.

2. Stability of this correlation against the detrimental effects of the UE.

Figs. 15, 16 and 17 allow for such comparisons.

In Fig. 15 we first revisit the case of the dilepton $t\bar{t}$ sample discussed in Sec. 4. In addition to the true $\sqrt{\hat{s}}$ (yellow shaded) and $\sqrt{\hat{s}}_{min}^{(reco)}$ (black) distribution already appearing in Fig. 3, we now also plot the distributions of $2M_{Tgen}$ (red dots), $H_T$ (green dots) and $\not{H}_T$ (blue dots), all calculated at the RECO-level. For completeness, in Fig. 15 we also show a variant of $M_{Tgen}$, called $M_{TTgen}$ (magenta dots), where all visible particle momenta are first projected on the transverse plane, before computing $M_{Tgen}$ in the usual way [32][14]. All results include the full simulation of the underlying event. For plotting convenience, the $\not{H}_T$ distribution is shown scaled down by a factor of 2.

[13] We caution the reader that $H_T$ is often defined in a more narrow sense than eq. (7.2). For example, sometimes the $\not{H}_T$ term is omitted, sometimes the sum in eq. (7.2) is limited to the reconstructed jets only; or to the four highest $p_T$ jets only; or to all jets, but starting from the second-highest $p_T$ one.

[14] We caution the reader that the definition of $M_{TTgen}$ cannot be found in the published version of Ref. [32] — the $M_{TTgen}$ discussion was added in a recent replacement on the archive, which appeared more than two years after the original publication.

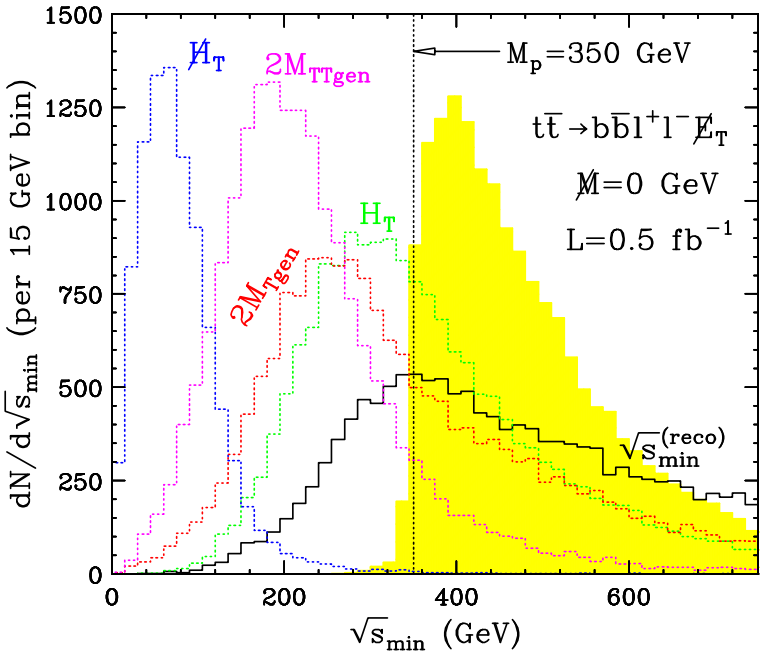


**Figure 15:** The same as Fig. 3, but now in addition to the true $\sqrt{s}$ (yellow shaded) and $\sqrt{s}_{min}^{(reco)}$ (black) distribution, we also plot the distributions of $2M_{Tgen}$ (red dots), $2M_{TTgen}$ (magenta dots), $H_T$ (green dots) and $\not{H}_T$ (blue dots), all calculated at the RECO-level. All results include the full simulation of the underlying event. For plotting convenience, the $\not{H}_T$ distribution is shown scaled down by a factor of 2. The vertical dotted line marks the $t\bar{t}$ mass threshold $M_p = 2m_t = 350$ GeV.

Based on the results from Fig. 15, we can now address the question, which inclusive distribution shows the best correlation with the parent mass scale (in this case the parent mass scale is the $t\bar{t}$ mass threshold $M_p = 2m_t = 350$ GeV marked by the vertical dotted line in Fig. 15). Let us begin with the two variables, $\not{H}_T$ and $H_T$, which do not depend on any unknown mass parameters. Fig. 15 reveals that the $\not{H}_T$ distribution peaks very far from threshold, and therefore does not reveal much information about the new physics mass scale. Consequently, any attempt at extracting new physics parameters out of the missing energy distribution alone, must make some additional model-dependent assumptions [72]. On the other hand, the $H_T$ distribution appears to correlate better with $M_p$, since its peak is relatively close to the $t\bar{t}$ threshold. However, this relationship is purely empirical, and it is difficult to know what is the associated systematic error.

Moving on to the variables which carry a dependence on a missing mass parameter, $\sqrt{s}_{min}^{(reco)}$, $2M_{Tgen}$ and $2M_{TTgen}$, we see that all three are affected to some extent by the presence of the UE. In particular, the distributions of $2M_{Tgen}$ and $2M_{TTgen}$ are now smeared and extend significantly beyond their expected endpoint (7.3). Not surprisingly, the UE has a larger impact on $2M_{Tgen}$ than on $2M_{TTgen}$. In either case, there is no obvious endpoint. Nevertheless, one could in principle try to extract an endpoint through a straight-line fit, for example, but it is clear that the obtained value will be wrong by a certain amount (depending

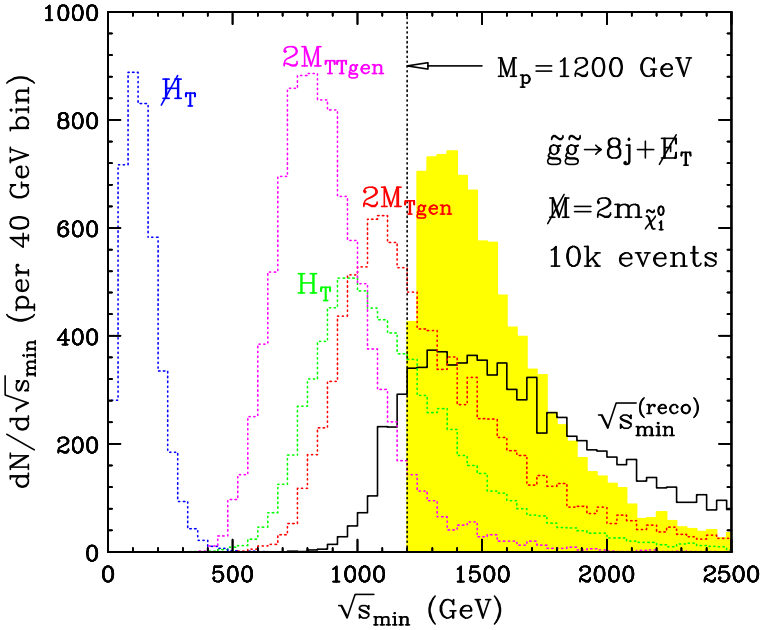


**Figure 16:** The same as Fig. 15, but for the gluino pair production example from Sec. 5, with each gluino decaying to 4 jets as in (5.1). We use the light SUSY mass spectrum from Fig. 10(a). The vertical dotted line now shows the $\tilde{g}\tilde{g}$ mass threshold $M_p = 2m_{\tilde{g}} = 1200$ GeV.

on the chosen region for fitting and on the associated backgrounds). All these difficulties with $2M_{Tgen}$ and $2M_{TTgen}$ are simply a reflection of the challenge of measuring a mass scale from an endpoint as in (7.3), instead of from a peak as in (4.7). By comparison, the determination of the new physics mass scale from the $\sqrt{s}_{min}^{(reco)}$ distribution is much more robust. As shown in Fig. 15, the $\sqrt{s}_{min}^{(reco)}$ peak is barely affected by the UE, and is still found precisely in the right location.

All of the above discussion can be directly applied to the SUSY examples considered in Sec. 5 as well. As an illustration, Figs. 16 and 17 revisit two of the gluino examples from Section 5. In both figures, we consider gluino pair-production with a light SUSY spectrum ($m_{\tilde{\chi}_1^0} = 100$ GeV, $m_{\tilde{\chi}_2^0} = 200$ GeV and $m_{\tilde{g}} = 600$ GeV). Then in Fig. 16 each gluino decays to 4 jets as in eq. (5.1), while in Fig. 17 each gluino decays to 2 jets as in eq. (5.2). (Thus Fig. 16 is the analogue of Fig. 10(a), while Fig. 17 is the analogue of Fig. 11(a).)

The conclusions from Figs. 16 and 17 are very similar. Both figures confirm that $\not{H}_T$ is not very helpful in determining the gluino mass scale $M_p = 2m_{\tilde{g}} = 1200$ GeV (indicated by the vertical dotted line). The $H_T$ distribution, on the other hand, has a nice well-defined peak, but the location of the $H_T$ peak always underestimates the gluino mass scale (by about 250 GeV in each case). Figs. 16 and 17 also confirm the effect already seen in Fig. 15: that the underlying event causes the $2M_{Tgen}$ and $2M_{TTgen}$ distributions to extend well beyond their upper kinematic endpoint, thus violating (7.3) and making the corresponding extraction of $M_p$ rather problematic. In fact, just by looking at Figs. 16 and 17, one might be tempted to

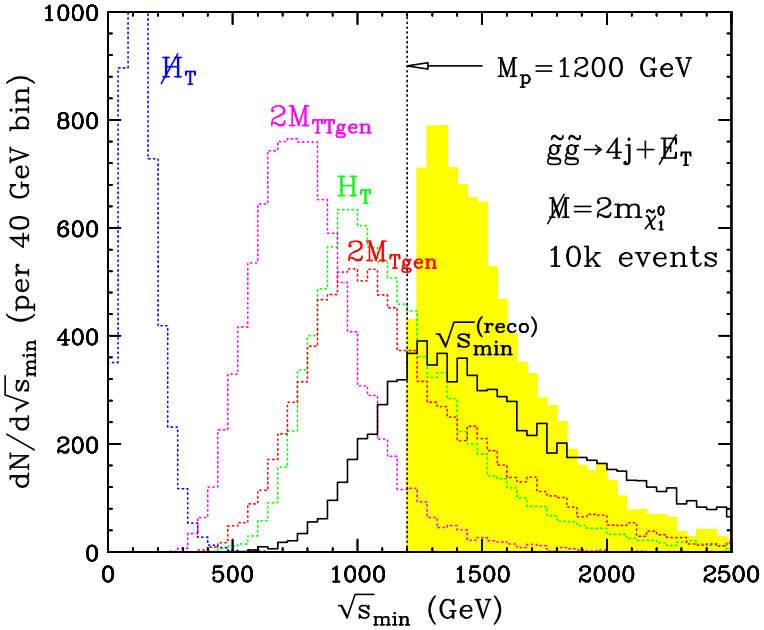


**Figure 17:** The same as Fig. 16, but with each gluino decaying to 2 jets as in (5.2). Compare to Fig. 11(a).

deduce that, if anything, it is the *peak* in $2M_{Tgen}$ that perhaps might indicate the value of the new physics mass scale and not the $2M_{Tgen}$ endpoint. Finally, the $\sqrt{s}^{(reco)}_{min}$ distribution also feels to some extent the effects from the UE, but always has its peak in the near vicinity of $M_p$. Therefore, among the five inclusive variables under consideration here, $\sqrt{s}^{(reco)}_{min}$ appears to provide the best estimate of the new physics mass scale. The correlation (4.7) advertized in this paper is seen to hold very well in Fig. 17 and reasonably well in Fig. 16.

## 8. Summary and conclusions

Since the original proposal of the $\sqrt{s}_{min}$ variable in Ref. [1], its practicability has been called into question in light of the effects from the underlying event, in particular initial state radiation and multiple parton interactions. In this paper we proposed two variations of the $\sqrt{s}_{min}$ variable which are intended to avoid this problems.

1. *RECO-level* $\sqrt{s}^{(reco)}_{min}$. The first variant, the RECO-level variable $\sqrt{s}^{(reco)}_{min}$ introduced in Sec. 2, is basically a modification of the *prescription for computing* the original $\sqrt{s}_{min}$ variable: instead of using (muon-corrected) calorimeter deposits, as was done in [1, 51], one could instead calculate $\sqrt{s}_{min}$ with the help of the reconstructed objects (jets and isolated photons, electrons and muons). Our examples in Sections 4, 5 and 6 showed that this procedure tends to automatically subtract out the bulk of the UE contributions, rendering the $\sqrt{s}^{(reco)}_{min}$ variable safe.

2. *Subsystem* $\sqrt{s}_{min}^{(sub)}$. Our second suggestion, discussed in Sec. 3, was to apply $\sqrt{s}_{min}$ to a *subsystem* of the observed event, which is suitably defined so that it does not include the contributions from the underlying event. The easiest way to do this is to veto jets from entering the definition of the subsystem. In this case, the subsystem variable $\sqrt{s}_{min}^{(sub)}$ is completely unaffected by the underlying event. However, depending on the particular scenario, in principle one could also allow (certain kinds of) jets to enter the subsystem. As long as there is an efficient method (through cuts) of selecting jets which (most likely) did not originate from the UE, this should work as well, as demonstrated in Fig. 6 with our $t\bar{t}$ example.

Being simply variants of the original $\sqrt{s}_{min}$ variable, both $\sqrt{s}_{min}^{(reco)}$ and $\sqrt{s}_{min}^{(sub)}$ automatically inherit the many nice properties of $\sqrt{s}_{min}$:

- Both $\sqrt{s}_{min}^{(reco)}$ and $\sqrt{s}_{min}^{(sub)}$ have a clear physical meaning: the minimum CM energy in the (sub)system, which is required in order to explain the observed signal in the detector.

- Both $\sqrt{s}_{min}^{(reco)}$ and $\sqrt{s}_{min}^{(sub)}$ are defined in a manifestly 1+3 Lorentz invariant way. As a consequence, their definitions utilize the available information about the longitudinal momentum components of the particles observed in the detector.

- Both $\sqrt{s}_{min}^{(reco)}$ and $\sqrt{s}_{min}^{(sub)}$ can be computed by simple analytical formulas, eqs. (2.13,2.14) and (3.5-3.8), correspondingly.

- $\sqrt{s}_{min}^{(reco)}$ (and to some extent $\sqrt{s}_{min}^{(sub)}$) is a general, global, and inclusive variable, which can be applied to *any* type of events, regardless of the event topology, number or type of reconstructed objects, number or type of missing particles, etc. For example, all of the arbitrariness associated with the number and type of missing particles is encoded by a *single* parameter $\not{M}$.

- The most important property of both $\sqrt{s}_{min}^{(reco)}$ and $\sqrt{s}_{min}^{(sub)}$ is that they exhibit a *peak* in their distributions, which *directly correlates* with the mass scale $M_p$ of the parent particles. In this regard we remind the reader that, compared to a kinematic endpoint, a peak is a feature which is much easier to observe and subsequently measure precisely over the SM backgrounds. This point was specifically illustrated in Sec. 7, where we contrasted the observability of the peak in the $\sqrt{s}_{min}^{(reco)}$ distribution to the observability of the endpoints of the $2M_{Tgen}$ and $2M_{TTgen}$ distributions.

At the same time, compared to the original calorimeter-based $\sqrt{s}_{min}$ variable considered in Ref. [1], the new variables $\sqrt{s}_{min}^{(reco)}$ and $\sqrt{s}_{min}^{(sub)}$ proposed here have one crucial advantage: they have very little sensitivity to the effects from the underlying event (ISR and MPI). As a result, the measurement of the corresponding mass scale from the peak in the distribution of $\sqrt{s}_{min}^{(reco)}$ or $\sqrt{s}_{min}^{(sub)}$ is robust and physically meaningful.

In conclusion, we have shown that the variables $\sqrt{s}_{min}^{(reco)}$ and $\sqrt{s}_{min}^{(sub)}$ have certain important advantages, and we feel that the experimental collaborations at the Tevatron and the LHC can only benefit from including them among their arsenal of observables.

## Acknowledgments

We thank A. Barr, C. Lester, F. Moortgat, L. Pape and B. Webber for stimulating discussions and correspondence. This work is supported in part by a US Department of Energy grant DE-FG02-97ER41029. SLAC is operated by Stanford University for the US Department of Energy under contract DE-AC02-76SF00515.

## References

[1] P. Konar, K. Kong and K. T. Matchev, "$\sqrt{\hat{s}}_{min}$ : A Global inclusive variable for determining the mass scale of new physics in events with missing energy at hadron colliders," JHEP **0903**, 085 (2009) [arXiv:0812.1042 [hep-ph]].

[2] S. Chang and A. de Gouvea, "Neutrino Alternatives For Missing Energy Events At Colliders," Phys. Rev. D **80**, 015008 (2009) [arXiv:0901.4796 [hep-ph]].

[3] A. J. Barr, B. Gripaios and C. G. Lester, "Transverse masses and kinematic constraints: from the boundary to the crease," JHEP **0911**, 096 (2009) [arXiv:0908.3779 [hep-ph]].

[4] P. Konar, K. Kong, K. T. Matchev and M. Park, "Dark Matter Particle Spectroscopy at the LHC: Generalizing MT2 to Asymmetric Event Topologies," JHEP **1004**, 086 (2010) [arXiv:0911.4126 [hep-ph]].

[5] K. Agashe, D. Kim, M. Toharia and D. G. E. Walker, "Distinguishing Dark Matter Stabilization Symmetries Using Multiple Kinematic Edges and Cusps," arXiv:1003.0899 [hep-ph].

[6] A. J. Barr and C. G. Lester, "A Review of the Mass Measurement Techniques proposed for the Large Hadron Collider," arXiv:1004.2732 [hep-ph].

[7] M. R. Buckley, H. Murayama, W. Klemm and V. Rentala, "Discriminating spin through quantum interference," Phys. Rev. D **78**, 014028 (2008) [arXiv:0711.0364 [hep-ph]].

[8] M. Burns, K. Kong, K. T. Matchev and M. Park, "A General Method for Model-Independent Measurements of Particle Spins, Couplings and Mixing Angles in Cascade Decays with Missing Energy at Hadron Colliders," JHEP **0810**, 081 (2008) [arXiv:0808.2472 [hep-ph]].

[9] F. Boudjema and R. K. Singh, "A model independent spin analysis of fundamental particles using azimuthal asymmetries," JHEP **0907**, 028 (2009) [arXiv:0903.4705 [hep-ph]].

[10] I. Hinchliffe, F. E. Paige, M. D. Shapiro, J. Soderqvist and W. Yao, "Precision SUSY measurements at LHC," Phys. Rev. D **55**, 5520 (1997) [arXiv:hep-ph/9610544].

[11] H. Bachacou, I. Hinchliffe and F. E. Paige, "Measurements of masses in SUGRA models at LHC," Phys. Rev. D **62**, 015009 (2000) [arXiv:hep-ph/9907518].

[12] I. Hinchliffe and F. E. Paige, "Measurements in SUGRA models with large tan(beta) at LHC," Phys. Rev. D **61**, 095011 (2000) [arXiv:hep-ph/9907519].

[13] B. C. Allanach, C. G. Lester, M. A. Parker and B. R. Webber, "Measuring sparticle masses in non-universal string inspired models at the LHC," JHEP **0009**, 004 (2000) [arXiv:hep-ph/0007009].

[14] B. K. Gjelsten, D. J. Miller and P. Osland, "Measurement of SUSY masses via cascade decays for SPS 1a," JHEP **0412**, 003 (2004) [arXiv:hep-ph/0410303].

[15] B. K. Gjelsten, D. J. Miller and P. Osland, "Measurement of the gluino mass via cascade decays for SPS 1a," JHEP **0506**, 015 (2005) [arXiv:hep-ph/0501033].

[16] A. Birkedal, R. C. Group and K. Matchev, "Slepton mass measurements at the LHC," *In the Proceedings of 2005 International Linear Collider Workshop (LCWS 2005), Stanford, California, 18-22 Mar 2005, pp 0210* [arXiv:hep-ph/0507002].

[17] D. J. Miller, P. Osland and A. R. Raklev, "Invariant mass distributions in cascade decays," JHEP **0603**, 034 (2006) [arXiv:hep-ph/0510356].

[18] D. Costanzo and D. R. Tovey, "Supersymmetric particle mass measurement with invariant mass correlations," JHEP **0904**, 084 (2009) [arXiv:0902.2331 [hep-ph]].

[19] M. Burns, K. T. Matchev and M. Park, "Using kinematic boundary lines for particle mass measurements and disambiguation in SUSY-like events with missing energy," JHEP **0905**, 094 (2009) [arXiv:0903.4371 [hep-ph]].

[20] K. T. Matchev, F. Moortgat, L. Pape and M. Park, "Precise reconstruction of sparticle masses without ambiguities," JHEP **0908**, 104 (2009) [arXiv:0906.2417 [hep-ph]].

[21] M. Burns, K. Kong, K. T. Matchev and M. Park, "Using Subsystem MT2 for Complete Mass Determinations in Decay Chains with Missing Energy at Hadron Colliders," JHEP **0903**, 143 (2009) [arXiv:0810.5576 [hep-ph]].

[22] M. M. Nojiri, G. Polesello and D. R. Tovey, "Proposal for a new reconstruction technique for SUSY processes at the LHC," arXiv:hep-ph/0312317.

[23] K. Kawagoe, M. M. Nojiri and G. Polesello, "A new SUSY mass reconstruction method at the CERN LHC," Phys. Rev. D **71**, 035008 (2005) [arXiv:hep-ph/0410160].

[24] H. C. Cheng, J. F. Gunion, Z. Han, G. Marandella and B. McElrath, "Mass Determination in SUSY-like Events with Missing Energy," JHEP **0712**, 076 (2007) [arXiv:0707.0030 [hep-ph]].

[25] M. M. Nojiri, G. Polesello and D. R. Tovey, "A hybrid method for determining SUSY particle masses at the LHC with fully identified cascade decays," JHEP **0805**, 014 (2008) [arXiv:0712.2718 [hep-ph]].

[26] H. C. Cheng, D. Engelhardt, J. F. Gunion, Z. Han and B. McElrath, "Accurate Mass Determinations in Decay Chains with Missing Energy," Phys. Rev. Lett. **100**, 252001 (2008) [arXiv:0802.4290 [hep-ph]].

[27] H. C. Cheng, J. F. Gunion, Z. Han and B. McElrath, "Accurate Mass Determinations in Decay Chains with Missing Energy: II," Phys. Rev. D **80**, 035020 (2009) [arXiv:0905.1344 [hep-ph]].

[28] B. Webber, "Mass determination in sequential particle decay chains," JHEP **0909**, 124 (2009) [arXiv:0907.5307 [hep-ph]].

[29] M. M. Nojiri, K. Sakurai and B. R. Webber, "Reconstructing particle masses from pairs of decay chains," arXiv:1005.2532 [hep-ph].

[30] C. G. Lester and D. J. Summers, "Measuring masses of semi-invisibly decaying particles pair produced at hadron colliders," Phys. Lett. B **463**, 99 (1999) [arXiv:hep-ph/9906349].

[31] A. Barr, C. Lester and P. Stephens, "m(T2): The truth behind the glamour," J. Phys. G **29**, 2343 (2003) [arXiv:hep-ph/0304226].

[32] C. Lester and A. Barr, "MTGEN : Mass scale measurements in pair-production at colliders," JHEP **0712**, 102 (2007) [arXiv:0708.1028 [hep-ph]].

[33] W. S. Cho, K. Choi, Y. G. Kim and C. B. Park, "Gluino Stransverse Mass," Phys. Rev. Lett. **100**, 171801 (2008) [arXiv:0709.0288 [hep-ph]].

[34] B. Gripaios, "Transverse Observables and Mass Determination at Hadron Colliders," JHEP **0802**, 053 (2008) [arXiv:0709.2740 [hep-ph]].

[35] A. J. Barr, B. Gripaios and C. G. Lester, "Weighing Wimps with Kinks at Colliders: Invisible Particle Mass Measurements from Endpoints," JHEP **0802**, 014 (2008) [arXiv:0711.4008 [hep-ph]].

[36] W. S. Cho, K. Choi, Y. G. Kim and C. B. Park, "Measuring superparticle masses at hadron collider using the transverse mass kink," JHEP **0802**, 035 (2008) [arXiv:0711.4526 [hep-ph]].

[37] H. C. Cheng and Z. Han, "Minimal Kinematic Constraints and MT2," JHEP **0812**, 063 (2008) [arXiv:0810.5178 [hep-ph]].

[38] K. T. Matchev, F. Moortgat, L. Pape and M. Park, "Precision sparticle spectroscopy in the inclusive same-sign dilepton channel at LHC," arXiv:0909.4300 [hep-ph].

[39] P. Konar, K. Kong, K. T. Matchev and M. Park, "Superpartner mass measurements with 1D decomposed MT2," arXiv:0910.3679 [hep-ph].

[40] D. R. Tovey, "On measuring the masses of pair-produced semi-invisibly decaying particles at hadron colliders," JHEP **0804**, 034 (2008) [arXiv:0802.2879 [hep-ph]].

[41] G. Polesello and D. R. Tovey, "Supersymmetric particle mass measurement with the boost-corrected contransverse mass," JHEP **1003**, 030 (2010) [arXiv:0910.0174 [hep-ph]].

[42] K. T. Matchev and M. Park, "A general method for determining the masses of semi-invisibly decaying particles at hadron colliders," arXiv:0910.1584 [hep-ph].

[43] T. Han, I. W. Kim and J. Song, "Kinematic Cusps: Determining the Missing Particle Mass at the LHC," arXiv:0906.5009 [hep-ph].

[44] A. Alves, O. Eboli and T. Plehn, "It's a gluino," Phys. Rev. D **74**, 095010 (2006) [arXiv:hep-ph/0605067].

[45] J. M. Butterworth, J. R. Ellis and A. R. Raklev, "Reconstructing sparticle mass spectra using hadronic decays," JHEP **0705**, 033 (2007) [arXiv:hep-ph/0702150].

[46] C. Csaki, J. Heinonen and M. Perelstein, "Testing Gluino Spin with Three-Body Decays," JHEP **0710**, 107 (2007) [arXiv:0707.0014 [hep-ph]].

[47] M. M. Nojiri, K. Sakurai, Y. Shimizu and M. Takeuchi, "Handling jets + missing $E_T$ channel using inclusive mT2," JHEP **0810**, 100 (2008) [arXiv:0808.1094 [hep-ph]].

[48] M. M. Nojiri, Y. Shimizu, S. Okada and K. Kawagoe, "Inclusive transverse mass analysis for squark and gluino mass determination," JHEP **0806**, 035 (2008) [arXiv:0802.2412 [hep-ph]].

[49] J. Alwall, K. Hiramatsu, M. M. Nojiri and Y. Shimizu, "Novel reconstruction technique for New Physics processes with initial state radiation," Phys. Rev. Lett. **103**, 151802 (2009) [arXiv:0905.1201 [hep-ph]].

[50] M. M. Nojiri and M. Takeuchi, "Study of the top reconstruction in top-partner events at the LHC," JHEP **0810**, 025 (2008) [arXiv:0802.4142 [hep-ph]].

[51] A. Papaefstathiou and B. Webber, "Effects of QCD radiation on inclusive variables for determining the scale of new physics at hadron colliders," JHEP **0906**, 069 (2009) [arXiv:0903.2013 [hep-ph]].

[52] A. Papaefstathiou and B. Webber, "Effects of invisible particle emission on inclusive variables for determining the scale of new physics at hadron colliders," arXiv:1004.4762 [hep-ph].

[53] G. Brooijmans *et al.*, "New Physics at the LHC. A Les Houches Report: Physics at TeV Colliders 2009 - New Physics Working Group," arXiv:1005.1229 [hep-ph].

[54] T. Hur, H. S. Lee and S. Nasri, "A Supersymmetric U(1)' Model with Multiple Dark Matters," Phys. Rev. D **77**, 015008 (2008) [arXiv:0710.2653 [hep-ph]].

[55] Q. H. Cao, E. Ma, J. Wudka and C. P. Yuan, "Multipartite Dark Matter," arXiv:0711.3881 [hep-ph].

[56] H. Sung Cheon, S. K. Kang and C. S. Kim, "Doubly Coexisting Dark Matter Candidates in an Extended Seesaw Model," Phys. Lett. B **675**, 203 (2009) [arXiv:0807.0981 [hep-ph]].

[57] T. Hur, H. S. Lee and C. Luhn, "Common gauge origin of discrete symmetries in observable sector and hidden sector," JHEP **0901**, 081 (2009) [arXiv:0811.0812 [hep-ph]].

[58] Greg Landsberg, "$\not\!\!E_T$ in CMS", talk given at the "Missing Energy" workshop, UC Davis, April 1, 2009.

[59] T. Sjostrand, S. Mrenna and P. Skands, "PYTHIA 6.4 physics and manual," JHEP **0605**, 026 (2006) [arXiv:hep-ph/0603175].

[60] J. Conway, "PGS: Simple simulation package for generic collider detectors," http://www.physics.ucdavis.edu/∼conway/research/software/pgs/pgs.html.

[61] G. L. Bayatian *et al.* [CMS Collaboration], "CMS physics: Technical design report," vol. I: "Detector Performance and Software", CERN/LHCC 2006-001.

[62] N. Kidonakis and R. Vogt, "The Theoretical top quark cross section at the Tevatron and the LHC," Phys. Rev. D **78**, 074005 (2008) [arXiv:0805.3844 [hep-ph]].

[63] P. Konar, K. Kong, K. T. Matchev, and M. Park, in preparation.

[64] https://twiki.cern.ch/twiki/bin/view/Main/SezenSekmen

[65] B. C. Allanach *et al.*, "The Snowmass points and slopes: Benchmarks for SUSY searches," in *Proc. of the APS/DPF/DPB Summer Study on the Future of Particle Physics (Snowmass 2001)* ed. N. Graf, Eur. Phys. J. C **25**, 113 (2002) [arXiv:hep-ph/0202233].

[66] K. Hamaguchi, E. Nakamura and S. Shirai, "A Measurement of Neutralino Mass at the LHC in Light Gravitino Scenarios," Phys. Lett. B **666**, 57 (2008) [arXiv:0805.2502 [hep-ph]].

[67] D. R. Tovey, "Measuring the SUSY mass scale at the LHC," Phys. Lett. B **498**, 1 (2001) [arXiv:hep-ph/0006276].

[68] J. Hisano, K. Kawagoe and M. M. Nojiri, "A detailed study of the gluino decay into the third generation squarks at the CERN LHC," Phys. Rev. D **68**, 035007 (2003) [arXiv:hep-ph/0304214].

[69] R. Kitano and Y. Nomura, "Supersymmetry, naturalness, and signatures at the LHC," Phys. Rev. D **73**, 095004 (2006) [arXiv:hep-ph/0602096].

[70] S. I. Bityukov and N. V. Krasnikov, "LHC (CMS) SUSY discovery potential for nonuniversal gaugino and squark masses and the determination of the effective SUSY scale," arXiv:hep-ph/0210269.

[71] A. J. Barr and C. Gwenlan, "The race for supersymmetry: using mT2 for discovery," Phys. Rev. D **80**, 074007 (2009) [arXiv:0907.2713 [hep-ph]].

[72] J. Hubisz, J. Lykken, M. Pierini and M. Spiropulu, "Missing energy look-alikes with 100 $\mathrm{pb}^{-1}$ at the LHC," Phys. Rev. D **78**, 075008 (2008) [arXiv:0805.2398 [hep-ph]].